



RICE UNIVERSITY

Stratospheric Scattering of
Radio Waves and the
Jicamarca Radio Telescope

by

Daniel Alfred Fleisch

A THESIS SUBMITTED
IN PARTIAL FULFILLMENT OF THE
REQUIREMENTS FOR THE DEGREE OF

MASTER OF SCIENCE

Thesis Director's Signature

A handwritten signature in cursive script, reading "A. E. Gordon", written over a horizontal line.

Houston, Texas
November, 1976

TABLE OF CONTENTS

	Page
INTRODUCTION	1
CHAPTER I	
1.1 Theory of Stratospheric Scattering	3
1.2 Description of Equipment and Procedures	10
1.3 Effect of Phase Oscillations on Data Analysis	15
CHAPTER II	
2.1 Current Antenna Beam Positions .	21
2.2 Improvement of the Vertical Beam	24
2.3 Error Due to Vertical Offset . .	33
APPENDIX	
One-dimensional Arrays (Unphased) . .	38
Two-dimensional Arrays (Unphased) . .	41
Phased Arrays	44
Partial Antenna Patterns.	63
BIBLIOGRAPHY	71

Phase Map List -

Phase Map I48
Phase Map II.60
Phase Map III60
Phase Map IV.37
Phase Map V37
Phase Map VI,37

Antenna Beam Map List -

Antenna Beam Map 1.30
Antenna Beam Map 2.31
Antenna Beam Map 3.32
Antenna Beam Map 4,67
Antenna Beam Map 5.68
Antenna Beam Map 6.70

Figure List -

Figure 1.111
Figure 1.218
Figure 2.123
Figure 2.225
Figure 2.334
Figure A-139
Figure A-242
Figure A-345
Figure A-451
Figure A-553
Figure A-657
Figure A-759
Figure A-861

STRATOSPHERIC SCATTERING OF RADIO WAVES
AND THE JICAMARCA RADIO TELESCOPE

by

Daniel Alfred Fleisch

ABSTRACT

Radar backscatter from the 15 to 35 km height range provides information about the dynamics and turbulent mixing of the stratosphere. The 3-dimensional space spectrum of turbulent fluctuations, the mean wind velocity, and the root-mean-square velocity fluctuations are directly related to the autocorrelation function of the scattered signals. The theory and mechanisms of stratospheric scattering of radio waves is discussed. The equipment and procedures used in previous experiments at the Jicamarca Radio Observatory are examined in detail, and are found to require modification in some cases. The theory of phased arrays is presented, and the correct and complete array factor pertinent to the Jicamarca antenna is derived. Information about the side lobes and precise positions of various beams is considered, and three beams are selected for use in a proposed stratospheric backscatter experiment. The phasing cables needed for the implementation of two off-vertical beams are available at the observatory, while new phasing cables must be manufactured for the realization of the vertical beam.

ACKNOWLEDGEMENTS

This work would not have been possible without the excellent guidance and patient support of Dr. W.E. Gordon. His help was always available but never forced upon me; the result is thesis which I feel represents my own work, with insight and direction provided by the years of experience of my advisor.

I also thank my wife Theresa Martin who supported me morally and financially during this work.

This research was funded through NSF Grant ATM75-19337.

INTRODUCTION

Signals scattered from dielectric fluctuations in the stratosphere contain much information about the scattering medium. The proposed experiment represents an attempt to discern from various aspects of these signals three important features of stratospheric composition and dynamics.

One interesting aspect of the returned signals is the power of the scattered radiation. The information contained in this quantity depends upon the primary mechanism by which scattering occurs. If particulate matter is present in sufficient quantities for the Rayleigh scattering process to contribute significantly to the signal, the scattered power is directly related to the number density of the particles. If eddy displacement is the primary scattering mechanism, the returned signal is related to the 3-dimensional space spectrum of the fluctuations, as discussed in Chapter 1.

Also of interest are the Doppler shift and spectral width of the scattered signals. These quantities provide information about the mean velocity of the scattering volume and the root mean square of velocity fluctuations, respectively (Derr, 1972). These are both important parameters in any theory of stratospheric dynamics and mixing (Webb, 1966).

The measurements will be made with the Jicamarca radio/radar telescope near Lima, Peru. The telescope consists of two superimposed arrays having orthogonal polarizations, and each consisting of 9216 half-wave dipoles. The tele-

scope will function as a 3-beam radar which will trace dielectric fluctuations of 3m wavelength. One beam will point directly vertically, a second will point approximately 3° off vertical to the south, and a third will be 3° off vertical to the west. The vertical beam will use all four quarters of one entire polarization, while the west and south beams will each utilize two adjacent quarters. The facilities now exist for the implementation of the two off-vertical beams, but the vertical beam requires the cutting of 56 new phase cables. Once installed, these cables will constitute a new pointing direction available to all users of the Jicamarca antenna, a direction which will be within 0.01° of true vertical and a considerable improvement over the current "vertical" pointing, which is offset from the true vertical by more than 1/3°.

CHAPTER I

1.1 Theory of Stratospheric Scattering

Radar study of the stratosphere in the height range of 15 to 35 km is a recent development. The initial attempt to detect backscatter from this region (Crane, 1970) yielded a signal marginally above the system sensitivity. More recently, workers at the Jicamarca Radio Observatory (JRO) in Peru have obtained signals from these heights which are some tens of dB above the noise level. The equipment and procedures used at JRO will be described later in this chapter. First the mechanism and theory of backscatter from the stratosphere will be explored.

An electromagnetic wave passing through any medium will have a small fraction of its energy scattered isotropically. This scattering is caused by dielectric constant fluctuations in the medium. In the stratosphere the intensity of the scattered waves is enhanced over the background "thermal" level through a process originally discussed by H. G. Booker and W. E. Gordon in 1957 (Booker and Gordon, 1957 and Gordon, 1958).

In that scheme, fluctuations of the dielectric constant occur whenever turbulence succeeds in producing eddies which are displaced while immersed in a dielectric constant gradient. Within these eddies conditions will be different from those of the surrounding medium, by an amount dependent on the vertical displacement and the gradient.

The refractive index "n" of a medium at radar wavelengths is a function of the temperature "T", pressure "p", and water vapor pressure "e" of the medium. The relationship is often expressed as

$$(n-1) \times 10^6 = \frac{79}{T}(p + \frac{4800e}{T}) \quad .$$

During the displacement process, an elementary volume within an eddy expands or contracts adiabatically, producing changes in p and T according to the formula

$$\frac{dT}{T} = \frac{\gamma-1}{\gamma} \frac{dp}{p}$$

where $\gamma = \frac{c_p}{c_v}$. The vertical displacement dz results in a pressure change $\frac{dp}{dz} = -\rho g$, where ρ is the density of air and $g = 9.8 \text{ m/s}^2$. Thus

$$\frac{dT}{T} = -\frac{\gamma-1}{\gamma} \frac{\rho g dz}{p}$$

or

$$\frac{dT}{dz} = -\frac{\gamma-1}{\gamma} \frac{\rho g}{p} T \quad .$$

But $\frac{\gamma-1}{\gamma} T \frac{\rho}{p} = \frac{1}{c_p}$,

so

$$\frac{dT}{dz} = -\frac{g}{c_p} = -\gamma_a$$

where γ_a is the well-known adiabatic lapse rate. Its value

is approximately $10^\circ/\text{km}$.

Integration of $\frac{dT}{dz}$ gives the quantity

$$\Theta = T + \gamma_a z$$

called the potential temperature and having the desirable quality of invariance within a volume as the volume changes height adiabatically.

Another quantity which varies as the volume expands or contracts is the water vapor pressure e . As the pressure p within the volume changes, e varies approximately as

$$e = 1.62 pq$$

where q is the specific humidity, defined as the ratio of the mass of water vapor to the mass of moist air in an elementary volume V . The quantity q , assuming no condensation, is also invariant within V during displacements.

We may therefore express the index of refraction n as

$$(n-1) \times 10^6 = \frac{79p}{\Theta - \gamma_a z} \left(1 + \frac{7800q}{\Theta - \gamma_a z}\right) .$$

Thus N , the refractive modulus, defined as $(n-1) \times 10^6$, is a function of z, p, Θ , and q , where the pressure, potential temperature, and specific humidity are also functions of z . If a parcel is displaced from z_1 to z_2 , the pressure within a volume changes from $p(z_1)$ to $p(z_2)$, while $\Theta(z_1)$ and $q(z_1)$

retain their values. The difference between the refractive modulus within the parcel and that of the surrounding air is then

$$\Delta N = N[z_2, p(z_2), \Theta(z_1), q(z_1)] - N[z_2, p(z_2), \Theta(z_2), q(z_2)]$$

The fluctuations are therefore characterized by the gradient

$$\frac{\partial N}{\partial z} = \frac{\partial N}{\partial \Theta} \frac{d\Theta}{dz} + \frac{\partial N}{\partial q} \frac{dq}{dz}$$

or

$$\begin{aligned} \frac{\partial N}{\partial z} &= \frac{79p}{(-\gamma_a z)^2} \left[\left(1 - \frac{2(7800q)}{(-\gamma_a z)}\right) \frac{dH}{dz} + 7800 \frac{dq}{dz} \right] \\ &= \frac{79p}{T^2} \left[\left(1 - \frac{2(7800q)}{T}\right) \left(\frac{dT}{dz} - \gamma_a\right) + 7800 \frac{dq}{dz} \right] . \end{aligned}$$

The quantities $\frac{q}{T}$ and $\frac{dq}{dz}$ are both extremely small, allowing us to write

$$\frac{\partial N}{\partial z} = \frac{79p}{T^2} \left[\frac{dT}{dz} + \gamma_a \right] .$$

In order to relate this expression for the fluctuation of the index of refraction to the signal received by a radar antenna illuminating a turbulent medium, it is necessary to understand the relationship between randomly varying functions, and the auto-correlation or structure functions characterizing the motions.

The space-time autocovariance function $\rho(\vec{r}, \tau)$ corresponding to the fluctuating index of refraction $n(\vec{x}, t)$ is

$$\rho(\vec{r}, \tau) = \langle n(\vec{x}, t) n(\vec{x} + \vec{r}, t + \tau) \rangle .$$

The radar equation may be used to determine the scattered field for such a medium. Wheelon (1959) gives an expression which, when adapted to the backscatter case, is

$$E_S(t) = (\pi \sqrt{P_T} \sin \chi / \lambda_0^2) e^{i \vec{k}_S \cdot \vec{O}\vec{R}} \int d^3 \vec{x} \frac{\exp[i \vec{x} \cdot \vec{k}_S] \delta n(\vec{x}, t)}{|\vec{R}|^2} \sqrt{\frac{G_T}{4\pi}}$$

where P_T = transmitted power, χ = polarization angle, λ_0 = radar wavelength, \vec{k}_S = Bragg vector, \vec{R} = distance between scattering element and radar, \vec{r} = distance between arbitrary origin within scattering volume and scattering element, and G_T = power gain along radar direction.

We now form the time correlation function $C(\tau) = \langle E_S(t) E_S^*(t + \tau) \rangle$:

$$C(\tau) = (\pi^2 P_T \sin^2 \chi / \lambda_0^4) \langle \iint d^3 \vec{x} d^3 \vec{x}' \frac{\exp[i(\vec{x} - \vec{x}') \cdot \vec{k}_S]}{4\pi G_T R^4} \delta n(\vec{x}, t)$$

$$\delta n(\vec{x}', t + \tau) \rangle .$$

Assuming that sufficient distance exists between the scattering element and the antenna to insure plane waves, the quantities G_T and R may be removed from the integrals, giving

$$C(\tau) = \left(\frac{\pi P_T \sin^2 \chi}{4 G_T R^4 \lambda_o^4} \right) \iint d^3 \vec{x} d^3 \vec{x}' \exp[i(\vec{x} - \vec{x}') \cdot \vec{o} \vec{k}_S] \langle \delta n(\vec{x}, t) \delta n(\vec{x}', t + \tau) \rangle.$$

Letting $\vec{x}' \rightarrow \vec{x} + \vec{r}$, this becomes

$$C(\tau) = \left(\frac{\pi P_T \sin^2 \chi}{4 G_T R^4 \lambda_o^4} \right) \iint d^3 \vec{x} d^3 \vec{r} \exp[-i \vec{k}_S \cdot \vec{o} \vec{r}] \langle \delta n(\vec{x}, t) \delta n(\vec{x} + \vec{r}, t + \tau) \rangle.$$

The integral over r is simply the Fourier transform of the autocovariance function of $\delta n(\vec{x}, t)$, since its argument is confined to a small volume of r -space, allowing extension of the limits to all space. We therefore have

$$C(\tau) = \frac{\pi P_T \sin^2 \chi}{4 G_T R^4 \lambda_o^4} V \rho(\vec{k}, \tau)$$

where

$$\rho(\vec{k}, \tau) = \int_{-\infty}^{\infty} d^3 \vec{r} \exp[-i \vec{k}_S \cdot \vec{o} \vec{r}] \langle \delta n(\vec{x}, t) \delta n(\vec{x} + \vec{r}, t + \tau) \rangle$$

or

$$\rho(\vec{k}, \tau) = \int_{-\infty}^{\infty} d^3 \vec{r} \exp[-i \vec{k}_S \cdot \vec{o} \vec{r}] \rho(\vec{r}, \tau).$$

Thus there is a direct connection between $\rho(\vec{k}, \tau)$, the 4-dimensional space-time spectrum of the fluctuating index of refraction, and $C(\tau)$, the time correlation function of the detected signal. The fact that $\rho(\vec{k}, \tau)$ plays a role indicates the dependence of the detected signal on the turbulence with wave numbers k_S , or $3m$ for Jicamarca parameters. There may exist turbulent fluctuations at various other wave numbers, but only those satisfying the Bragg condition contribute to $C(\tau)$.

The relation of the 4-dimensional space-time spectrum $\rho(\vec{k}, \tau)$ to the previously calculated turbulence-induced gradient of the index of refraction is provided by Tatarski (1961). Using turbulence theory presented by Obukhov (1949), Tatarski derives the three-dimensional space spectrum of the refractive index fluctuations as

$$\phi_n(\vec{k}) = 0.033 c_n^2 k^{-11/3}$$

where

$$c_n = a L_0^{2/3} \frac{\partial N}{\partial z} .$$

In this equation L_0 represents the largest scale size of the turbulent eddies, a is a constant "near unity", and $\frac{\partial N}{\partial z}$ is the expression derived above for refractive index fluctuations. Thus

$$\phi_n(\vec{k}) = 0.033 a^2 L_0^{4/3} \left[\frac{79p}{T^2} \left(\frac{\partial T}{\partial z} + \gamma_a \right) \right]^2 k^{-11/3} .$$

In the notation utilized above, $\phi_n(\vec{k})$ corresponds to $\rho(\vec{k}, 0)$, establishing the connection between $\frac{\partial N}{\partial z}$ and the scattered signal. Woodman and Guillen (1974) experimentally deduced L_0 to be ~ 100 m, although the data does not appear to be entirely self-consistent. The equipment and procedures pertinent to the Jicamarca stratospheric backscatter experiments will be discussed 1.2a.

1.2 Description of Equipment and Procedures

The Jicamarca radio telescope is located 25 km north-east of Lima, Peru, at latitude $11^{\circ}57'$ south, longitude $76^{\circ}52'$ west. The antenna consists of 2 superimposed orthogonal arrays each containing 9216 half-wave dipoles, and operates at a wavelength of approximately 6 meters. The arrays are flat, square, and 291 meters on each side. When the telescope was constructed in 1960, one diagonal lay along the magnetic meridian, 6.01° east of geographic north. The dipole centers are separated by 3m, and are supported 1.8m above a reflecting plane. Each array has its dipoles at right angles to those of the other; independent feed lines to the two arrays allow a variety of polarizations to be synthesized.

The antenna is divided into four quarters, as seen in Fig. 1-1. Each dashed line represents two 6-inch diameter feed lines which connect each quarter to the transmit-receive systems. Each quarter is further divided into 16 "modules", represented by dots in Fig. 1-1. A module is a collection of 288 dipoles, 144 of each polarization. The modules are fed through equal lengths of 6-inch transmission line from the center of each quarter. It is at the connection points between these lines and each module that lengths of RG-17 cable may be used to achieve a phase shift between modules.

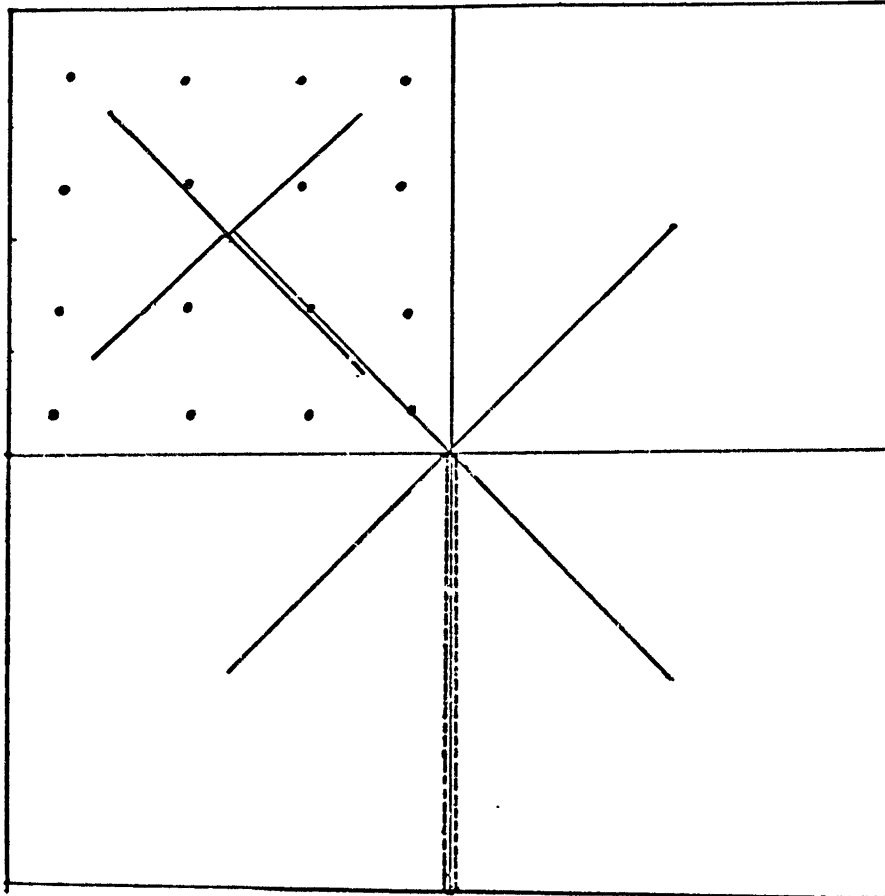


Figure 1-1

Transmitter and Receiver Systems

Generation of the signal is accomplished through the use of a .9984 MHz master oscillator and a x50 frequency multiplier, producing a 49.92 MHz signal. Intermediate and final power amplifier tubes increase the signal to a 1.5 Mw maximum. A total of four such generators are available.

The transmitter is pulsed to produce pulses of various lengths and periods as controlled by a digital correlator. Prevention of receiver and/or antenna loading during improper portions of the cycle is accomplished through the use of transmit-receive (TR) switches.

The receiver system entails one receiver for each independent antenna section. The optimum configuration for measuring three vector wind components is shown in the Appendix to consist of four quarters, all of one linear polarization, looking along the vertical, with the other linear polarization divided in half along a NE_m-SW_m line. Two quarters then look south, and the other two west. The number of receivers required is thus 3 in this case.

Detection and amplification of the 49.92 MHz signal occurs in two stages. Initially, a local oscillator produces a signal at 54.67 MHz which is mixed with the detected signal to yield 4.75_{\pm} MHz, where the \pm indicates the Doppler shift of the detected signal. Another local oscillator produces a 5.205 MHz signal, which, when mixed with 4.75_{\pm} MHz, gives a $455_{\bar{+}}$ kHz output.

Meanwhile, the 0.9984 MHz master oscillator and the 54.67 local are beat to produce a reference 4.75 MHz signal. This is mixed with the 5.205 MHz LO signal to produce a 455 kHz reference signal. Two phase detectors are then used to determine the two components of the signal which will become the real and imaginary portions of the auto-correlation function. These are evaluated with respect to the 455 kHz reference signal and digitized via analog-to-digital converters. Block diagrams of the transmitter and receiver systems may be found in Rastogi (1975), upon which these descriptions are based.

The autocorrelation function may be estimated through the following signal-processing procedure. N_1 pulses are transmitted at a given pulse length (PL) and separated by some inter-pulse period (IPP). The receiver is turned on after some gate delay (GD) dictated by the height region to be studied, which is $h = \frac{c(GD)}{2}$. The receiver is on for a period called the gate width (GW).

If we denote the sine and cosine outputs of detectors for the n^{th} pulse by x_n and y_n , the coherent averages of the received pulses from the first series of transmitted pulses are \bar{x}_1 and \bar{y}_1 , where

$$\bar{x}_1 = \frac{1}{N_1} \sum_{n=1}^{N_1} x_n \quad \text{and} \quad \bar{y}_1 = \frac{1}{N_1} \sum_{n=1}^{N_1} y_n .$$

The averaging is done in the digital correlator for a period of length $\tau = N_1(IPP+GW)$. The samples are then put

in the complex form $\bar{z}_1 = \bar{x}_1 + i\bar{y}_1$. N_2 of these samples are coherently averaged to provide an estimate of the complex autocorrelation function for various time lags.

The phase ϕ_N of the autocorrelation function is determined from the real and imaginary parts of that function. For example, if G_1 and G_2 are the complex signals received from two pulses in the k^{th} sample, we may write

$$G_1 = x_{1k} - iy_{1k}$$

and

$$G_2 = x_{2k} - iy_{2k} .$$

The imaginary part of the autocorrelation function is now

$$a_{N_2} = \frac{1}{N_2} \sum_{k=1}^{N_2} (x_{1k} y_{2k} - x_{2k} y_{1k})$$

while the real part is

$$b_{N_2} = \frac{1}{N_2} \sum_{k=1}^{N_2} (x_{1k} x_{2k} - y_{1k} y_{2k}) .$$

The phase of the autocorrelation function for these N_2 sample pairs is then just

$$\phi_{N_2} = \tan^{-1}(a_{N_2}/b_{N_2}) .$$

The mean wind speed and turbulent velocity fluctuations are obtained through analysis of the power spectrum of the scattered signal. The Doppler shift of the signal is related to the mean wind velocity through the relation

$$\Omega = -\vec{k}_s \cdot \vec{v}$$

where Ω is the Doppler frequency shift and \vec{k}_s is the Bragg vector. The spectrum is broadened by, among other things, the random Doppler shifts of individual scattering elements. The spectrum width is related to the variance of the random velocity fluctuations by the formula

$$\sigma = \frac{2\omega_0 \langle \Delta N^2 \rangle^{1/2}}{c}$$

where $\omega_0 = 50$ MHz and $c = 3 \times 10^8$ m/x. These quantities have been estimated in the past through consideration of the autocorrelation function at only 3 time lags, as will be discussed in the next section.

1.3 Effect of Phase Oscillations on Data Analysis

In previous stratospheric wind measurements (Woodman and Guillen, 1974), as well as many mesospheric experiments (Rastogi, 1975), the complex autocorrelation function and the phase were estimated at only three time lags. This follows the method of measuring vertical F-region drifts (Woodman and Hagfors, 1969) with a minimum of on-line computation. This method relies on a Fourier transform theorem which relates moments of a power spectrum to derivatives of the autocorrelation function. For example, the Doppler shift of the signal is found from the first moment of the

power spectrum $S(\omega)$

$$\Omega = \int_{-\infty}^{\infty} \omega S(\omega) d\omega$$

where $S(\omega) = \int_{-\infty}^{\infty} C(\tau) e^{-i\omega\tau} d\tau$. This same information is contained in the first derivative of the autocorrelation function, $C(\tau)$, or, equivalently, the first derivative of the phase ϕ_N evaluated at $\tau = 0$

$$v = -ik^{-1} \left\{ \frac{C'(0)}{C(0)} \right\} = k^{-1} \phi'_N(0)$$

Now at some small lag δ , assuming $\phi(0) = 0$, we have

$$\phi'(0) \approx \frac{\phi(\delta) - \phi(0)}{\delta} = \frac{\phi(\delta)}{\delta} .$$

Thus

$$v = k^{-1} \left\{ \frac{\phi(\delta)}{\delta} \right\} .$$

This approximation requires sufficiently small δ such that higher orders in a Taylor expansion of ϕ are negligible.

In the simple case of scattering from a medium moving with velocity \vec{v} , the power spectrum will be Doppler shifted by an amount

$$\Omega = -\vec{k}_s \cdot \vec{v}$$

where $\vec{k}_s \cdot \vec{v}$ is the component of v in the radar direction.

The autocorrelation function $C(\tau)$ may then be written

$$C(\tau) = A(\tau)e^{i\omega\tau}$$

thus indicating the linearity of $\phi(\tau)$ with τ .

However, the actual scattering volume in the stratosphere may not behave in this simple manner. Some experimental results reveal an oscillation of the phase values about a linear component, as illustrated in Fig. 1-2. This feature may indicate the presence of more than one component within the scattering volume, as will be discussed shortly. Whatever physical mechanism is responsible for this effect, it represents serious problems for the method of determining \vec{v} outlined above. This is most easily seen by considering point 1 in Fig. 1-2. If this point, representing $\phi(\tau)$ at lag τ , were chosen to calculate the slope at $\tau = 0$, the results would be quite different from those attained using the value of $\phi(\tau)$ corresponding to 1'. Choosing larger values of σ might avoid this problem, but this improvement is gained at the expense of the validity of the relation $\phi(\tau) = \phi'(0)\tau$. For this reason, more points must be considered in evaluating the autocorrelation function and its phase. Apparently, the improved computing capabilities of the Datacraft computer now available at JRO have obviated the need for this time-saving approximation.

Even if this problem in the estimation of wind velocities is avoided by using more complete data-taking procedures, the phase-oscillation phenomenon is a real feature of the data, and as such may contain information

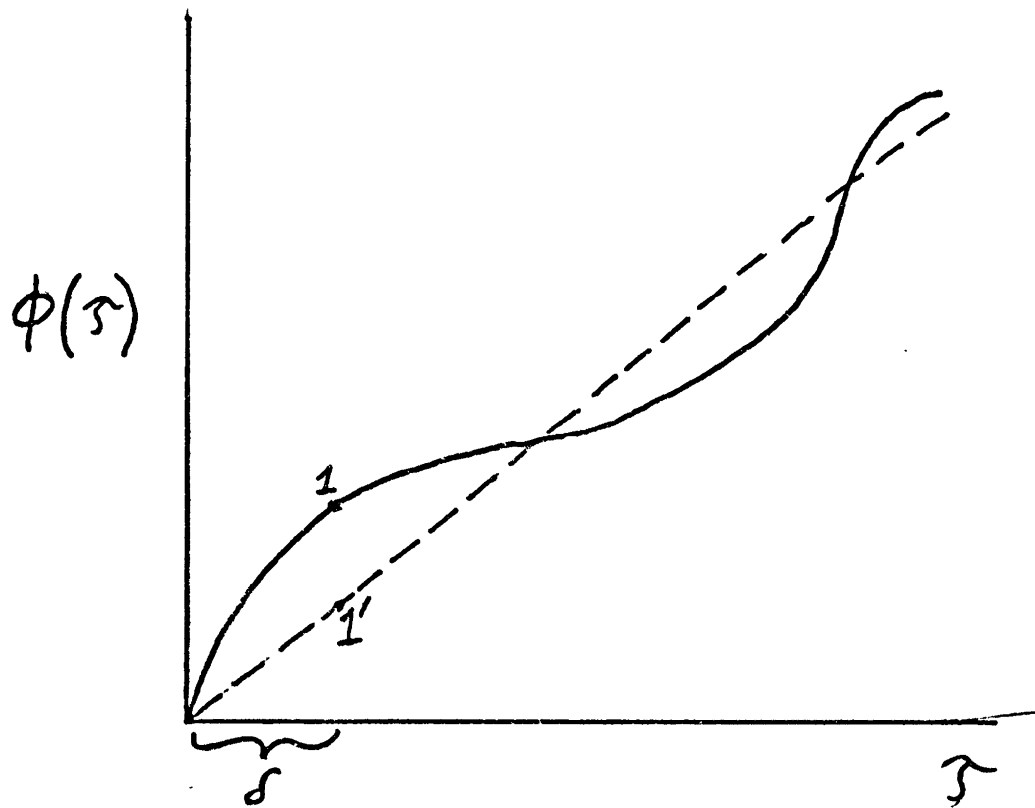


Figure 1-2

about the processes occurring within the scattering volume. Although this problem is largely untreated in the literature, those workers who do address the question generally attribute the non-linearity of the phase to the presence of more than one layer within the scattering volume (Rastogi, 1975; Misener, private communication). This conclusion is a result of an analysis of the relative contributions of two scattering layers, each of which produces a Gaussian power spectrum of the form

$$F_0(\nu) = A e^{-C \frac{\nu^2}{\sigma^2}}$$

where σ = half-width at half power.

The autocorrelation function corresponding to this power spectrum is

$$F_0(\tau) = A' e^{-C' \sigma^2 \tau^2} .$$

If $F(\nu)$ is shifted from the origin by an amount ν_1 , its Fourier transform is shifted by

$$F_{\nu_1}(\tau) = F_0(\tau) e^{-2\pi i \nu_1 \tau} .$$

The autocorrelation function representing the contributions of two such layers is then

$$\rho(\tau) = A'' e^{-(C'_1 \sigma_1^2 \tau^2 + 2\pi i \nu_1 \tau)} + B'' e^{-(C'_2 \sigma_2^2 \tau^2 + 2\pi i \nu_2 \tau)} .$$

The behavior of this function and its phase $\phi(\tau)$ is fairly sensitive to changes in σ_1 , σ_2 , v_1 , v_2 , A'' and B'' . However, reasonable values of these variables do indeed yield phase oscillations similar to those depicted in Fig. 1-2. The damping of the oscillations with increasing τ is present in the 2-layer model as well as some of the experimental data, but it is not clear that this behavior is a permanent feature of all the stratospheric data. This aspect of remote sensing of stratospheric winds certainly deserves more attention in future experiments.

CHAPTER II

Improvements on Previous Experiments

In attempting to resolve three vector components of the stratospheric winds, it is vital to know the pointing direction of the various radar beams as accurately as possible. Knowledge of these pointing directions allows the experimenter to analyze the contributions of various wind components to the signal detected from each beam. This chapter relates the results of the calculations contained in the Appendix to various antenna configurations currently in use at JRO, and considers improvements which are necessary and desirable for a 3-component stratospheric wind experiment.

2.1 Current Antenna Beam Positions

The position of the center of the Jicamarca beam which is perpendicular to the plane of the antenna (the unphased pointing direction) has been shown by antenna surveys and radio star calibration to have declination $\delta = -12.88^\circ$ and hour angle $HA = 4^m 37^s$ West. The zenith distance generally found in the literature for this direction is $z = 1.50^\circ$. However, using the formulae

$$\cos z = \sin \delta \sin \phi + \cos \delta \cos \phi \cos HA$$

and

$$\sin Az = \frac{\cos \delta \sin HA}{\sin z}$$

where z is the zenith distance, δ is the declination, ϕ is the latitude, HA is the hour angle, and Az is the azimuth (proceeding west of south), we find $z = 1.46^\circ$, and $Az = 50.35^\circ$. Here ϕ is -11.95° , the latitude of JRO.

The beam is thus 1.46° away from the local zenith, and any attempt to look in the vertical direction must involve phasing the array by the proper amount to correct for this offset. Notice that the phasing need only be along one axis of the array due to (perhaps fortuitous) geometric considerations (see Figure 2-1). The error introduced by one-axis phasing toward the zenith results in an offset from the true zenith of approximately 0.01° .

Using $z = 1.46^\circ$, $Az = 50.35^\circ$ as a starting point, along with the array theory discussed in the Appendix, the net effect of the current phasing configurations as well as the phasing needed to bring the beam into a truly vertical direction may be computed.

Two positions of extreme importance in stratospheric scattering experiments are those labeled "1" and "3" in Rastogi (1975), reported there to have $\delta = 11.78^\circ$ and $Ha = -14^m 19^s$ for position 1 and $\delta = -15.49^\circ$, $HA = -2^m 20^s$ for 3. In fact, the phasing schemes used by Rastogi, designated positions II and III in the Appendix, are shown to move the beam 2.31° along the magnetic (1960) EW axis, and 1.10° along the magnetic NS axis. The results are illustrated in Figure 2.2. Position 1 is found to have $z = 3.44^\circ$, $Az = 92.9^\circ$, while position 3 has $z = 3.46^\circ$, $Az = 8.83^\circ$.

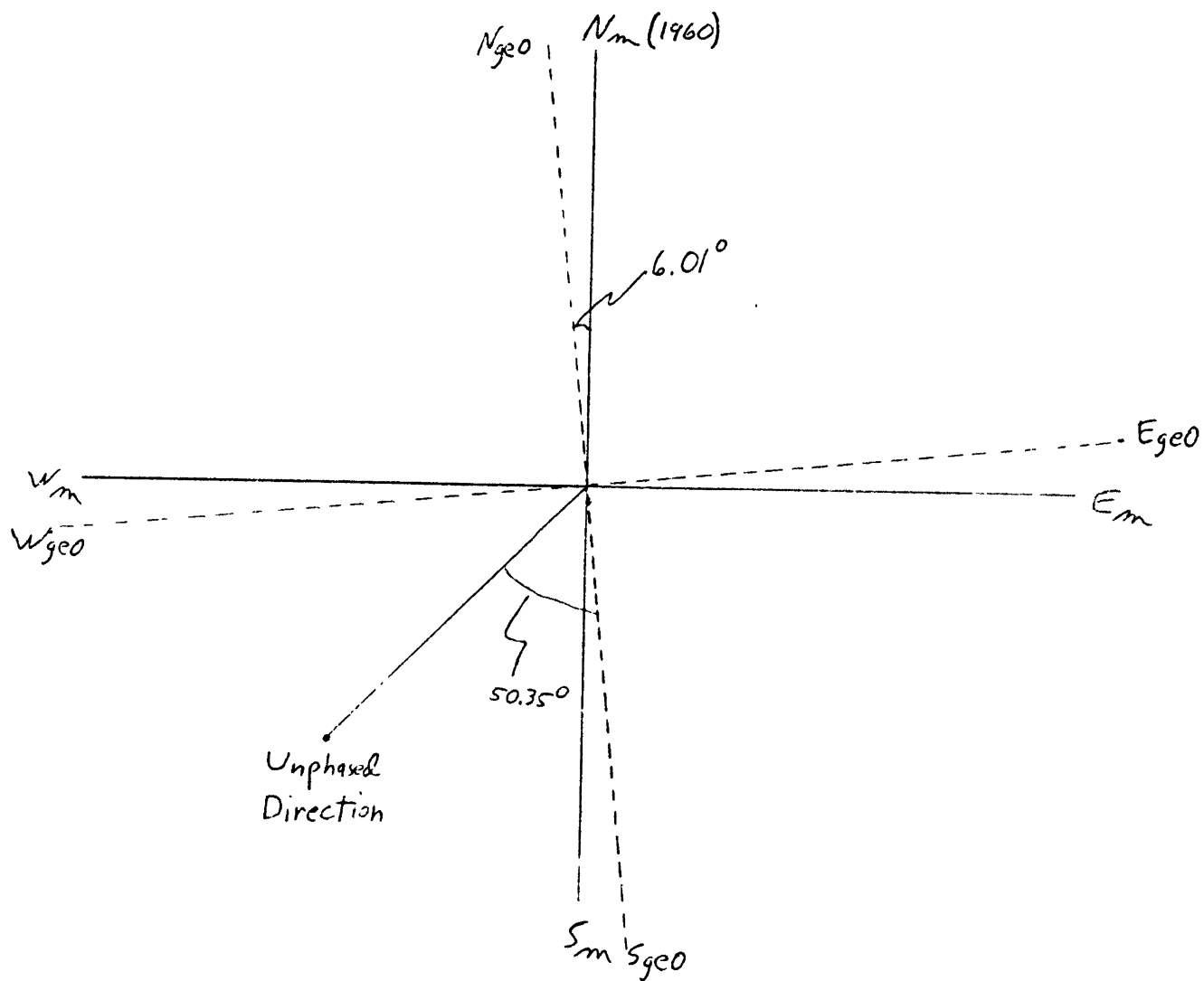


Figure 2-1

To convert this to declination and hour angle, we use the formulae

$$\sin\delta = \sin\phi \cos z - \cos\phi \sin z \cos Az$$

$$\sin HA = \frac{\sin z \sin Az}{\cos\delta}$$

Position 1 thus has $\delta = -11.75^\circ$, $HA = -14^m 02^s$, position 3 has $\delta = -15.37^\circ$, $HA = -2^m 12^s$.

Knowing the true positions of beams produced by phase maps II and III would allow us to compute the necessary phasing to put the beams exactly on the West and South axes. The azimuth of position 1 is within 3° of the West axis, and position 3 is within 9° of the South axis. The horizontal winds may be accurately resolved with current phase schemes; however, there exist important considerations on behalf of aligning the "vertical" radar beam exactly with the true vertical, as will be discussed in the remainder of this chapter.

2.2 Improvement of the Vertical Pointing

A very important position in stratospheric wind experiments is the so-called "vertical" pointing, corresponding to phase map I of the Appendix. In 1965, Ochs determined this position to have $\delta = 12.13^\circ$, $HA = 0^m 55^s$ West, having used an unphased zenith distance of 1.50° and the simplified "uniform phase gradient" calculation. This left the beam

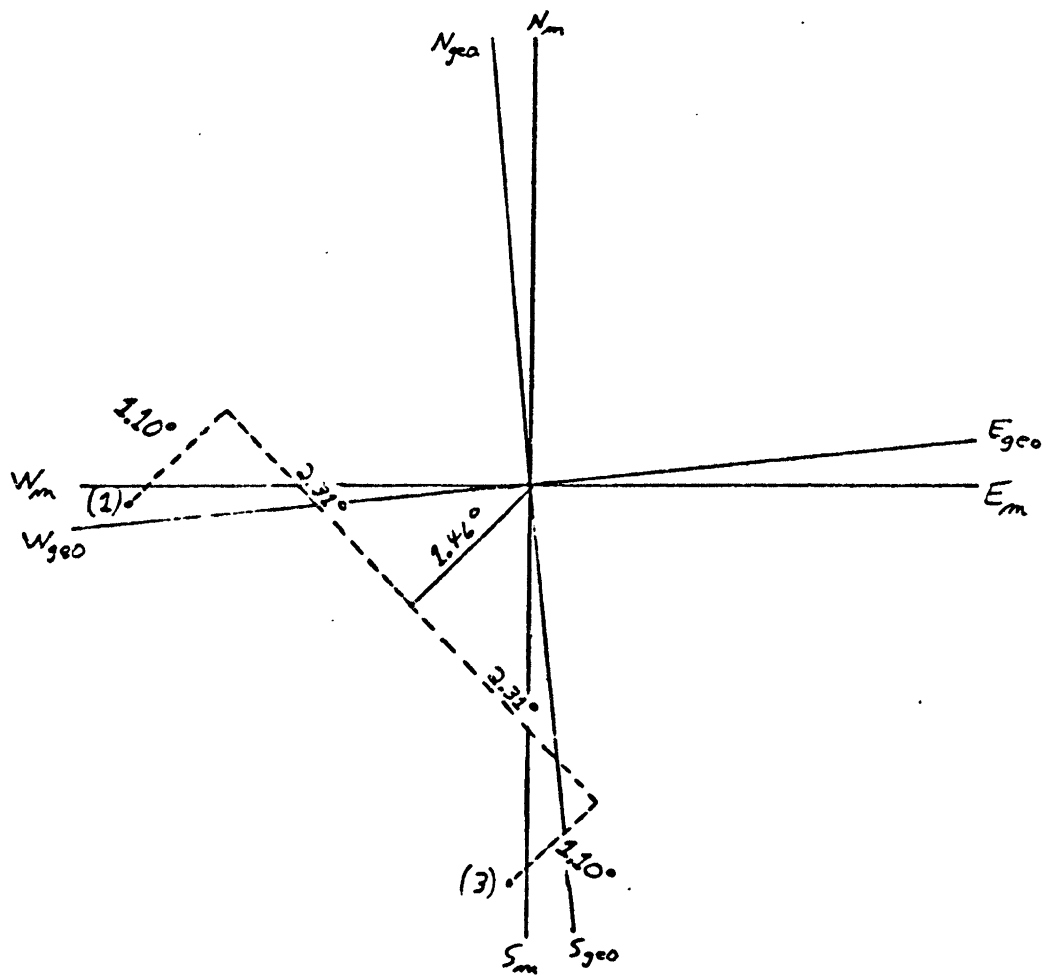


Figure 2-2

center 0.31° from the local zenith. In 1975 Rastogi used a closer value of 1.48° for the zenith distance of the unphased pointing direction, leaving 0.29° as the zenith distance of the phased "vertical" pointing. However, the complete array calculation, as presented in the Appendix, shows that the beam moves only 1.10° using phase map I, leaving the beam with zenith distance $z = 0.36^\circ$. The undesirability of such a tilt will be demonstrated below.

In order to correct the vertical pointing to $z = 0.0^\circ$, additional phasing is necessary. The most obvious method of accomplishing the desired correction is to simply increase the cable insertions in the current scheme by a factor of

$$\frac{\text{desired beam shift}}{\text{current beam shift}} = \frac{1.461}{1.101} = 1.327 \quad .$$

The phase map resulting from this addition is given as Phase Map IV at the end of this chapter.

Computer evaluation of the array factor with this phasing configuration shows the maximum is indeed shifted by 1.46° from the unphased direction. Thus the beam maximum is within 0.01° of the true zenith, the slight offset being due to the azimuthal difference between the direction the beam is moving and the direction directly toward the zenith (see Figure 2-1). This is one possible solution to the vertical offset problem.

Another simple method of increasing the beam shift from 1.10° to the desired 1.46° is the insertion of additional

cable length at the level of antenna quarters, each of which is a square array of 16 modules (Figure A-5). In this configuration, the relative phase between modules is identical to that currently used, but additional cable is inserted in the feed lines to the various quarters of the array. In essence, this method alters only the "quarter" array sub-factors discussed in the Appendix, rather than both the "quarter" and "module" sub-factors as in the previous case.

The additional cable insertions may no longer be computed by the simple "desired/achieved" ratio as above, since the "achieved" portion of that fraction was accomplished through phasing at a lower level, i.e., the modules. Trial and error reveals the correct factor for increased cable insertions at the "quarter" level to be 1.41. The phase map is therefore unchanged from the current "vertical" case, but now the signal from the North and East quarters traverses cables which are longer than those leading to the South and West quarters by a factor of 1.41.

Evaluation of the new array factor reveals a maximum at 1.46° . However, as might be expected when phasing is performed at a higher level, side-lobe problems must be considered. As noted in the Appendix, the sub-factors which multiply to make up the complete array factor may combine in curious ways. An examination of these combinations reveals side-lobe information.

The side lobes of interest are those on the axis along which the phasing is done. On this axis, the side lobe "beyond" the main beam (i.e., the lobe farther from the starting point) is generally found to be suppressed. For example, if the additional phasing is done by increasing the current phasing as described above, this lobe is 34 dB* below the main lobe. In the case of phasing at the "quarter" level, the lobe is more pronouncedly suppressed, and is 48 dB below the main lobe.

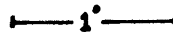
The side lobes on the opposite side of the main lobe display the opposite behavior, and it is the first lobe on this side that is enhanced by higher-level phasing. In the case of increasing current phasing, that is, phasing at successive pairs of modules, this lobe is 20 dB below the main lobe. However, if the phasing is performed at the level of the quarters, this lobe is only 9 dB below the main lobe. In both cases, the next appreciable lobe on this side of the main lobe is 10-11 dB below the main. These lobes are located 4.36° away from beam center, however, and are therefore less troublesome than those previously discussed. It may be noted that this lobe is actually larger than the first side lobe in one case, a consequence of the peculiar results attainable in multiplication of the subfactors.

*All dB are radar decibels.

Thus, the greatest effect of phasing at the level of the quarters rather than the pairs of modules is the enhancement of the first side lobe on one side of the main lobe by 11 dB, leaving it only 9 dB below the main lobe. At 1.48° from beam center, this represents a large enough contribution to the signal to warrant its avoidance. The advantage of phasing at the "quarter" level is that additional cable need only be inserted at 2 points, both within the switchyard near the control building. Additional phasing performed at the level of module pairs requires cable insertions at each of 56 modules, with successive modules receiving equal lengths of extra cable.

However, as long as each module requires extra cable, there is no justification for continuing the practice of combining pairs of modules as depicted by phase map IV. A preferable procedure would be to increase the cable insertions between each module, with cable lengths corresponding to phase map V. The advantages of this scheme may be seen by considering Antenna Beam Maps 1 through 3. These maps show the array-factor amplitudes for the main beam and important side lobes for the three methods of achieving true vertical outlined above. Maps 1 and 2 depict the lobe information for additional phasing done at the module pair and quarter level, respectively, while map 3 gives the values achieved when a phase gradient is inaugurated between each module and the next. This method clearly provides the most desirable main-to-side lobe ratio, although the same

•1880
(-25dB)



•184
(-65dB)

•1100
(-34dB)

•927
(-37dB)

•1785
(-26dB)

Zenith 0 7763
(0dB)

•1785
(-26dB)

•927
(-37dB)

•799
(-40dB)

x Normal to Array

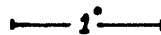
•2505
(-20dB)

•2072
(-23dB)

•4274
(-10dB)

Antenna Beam Map 1

•1845
(-24dB)



•70
(-81dB)

•487
(-47dB)

•464
(-48dB)

•894
(-37dB)

•1720
(-26dB)

Zenith 7484
(0dB)

•1720
(-26dB)

•894
(-37dB)

•770
(-40dB)

xNormal to Array

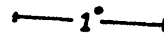
•4422
(-9dB)

•724
(-41dB)

•4051
(-11dB)

Antenna Beam Map 2

•715
(-44dB)



•850
(-41dB)

•1931
(-26dB)

•1056
(-37dB)

•2032
(-26dB)

Zenith 08840
(0dB)

•2032
(-26dB)

•1056
(-37dB)

•910
(40dB)

*Normal to Array

•2122
(-25dB)

•1287
(-33dB)

•1107
(-36dB)

Antenna Beam Map 3

number of cable insertions (56) is required as in the module pair method.

It should be noted that all of the procedures just discussed for correction of the vertical pointing have involved addition of extra cable to the existing phasing schemes. An alternative procedure would consist of deletion of sections of cables in proper amounts to achieve the same result. The phase map required for this configuration is designated phase map VI at the end of this chapter.

2.3 Error Due to Vertical Offset

The current offset of 0.36° of the "vertical" pointing from the true vertical may not seem, at first glance, to warrant the time and expense involved in implementing the corrections discussed above. However, an examination of the geometry pertinent to the stratospheric scattering experiments reveals that even so small an offset as 0.36° may result in considerable error in the estimation of various wind components. The geometry is illustrated in Figure 2.3.

The wind vector, V , is given by

$$\vec{V} = u\hat{x} + v\hat{y} + w\hat{z}$$

while the radar vector, R , is

$$\vec{R} = \sin\psi \cos\alpha \hat{x} + \sin\psi \sin\alpha \hat{y} + \cos\psi \hat{z} .$$

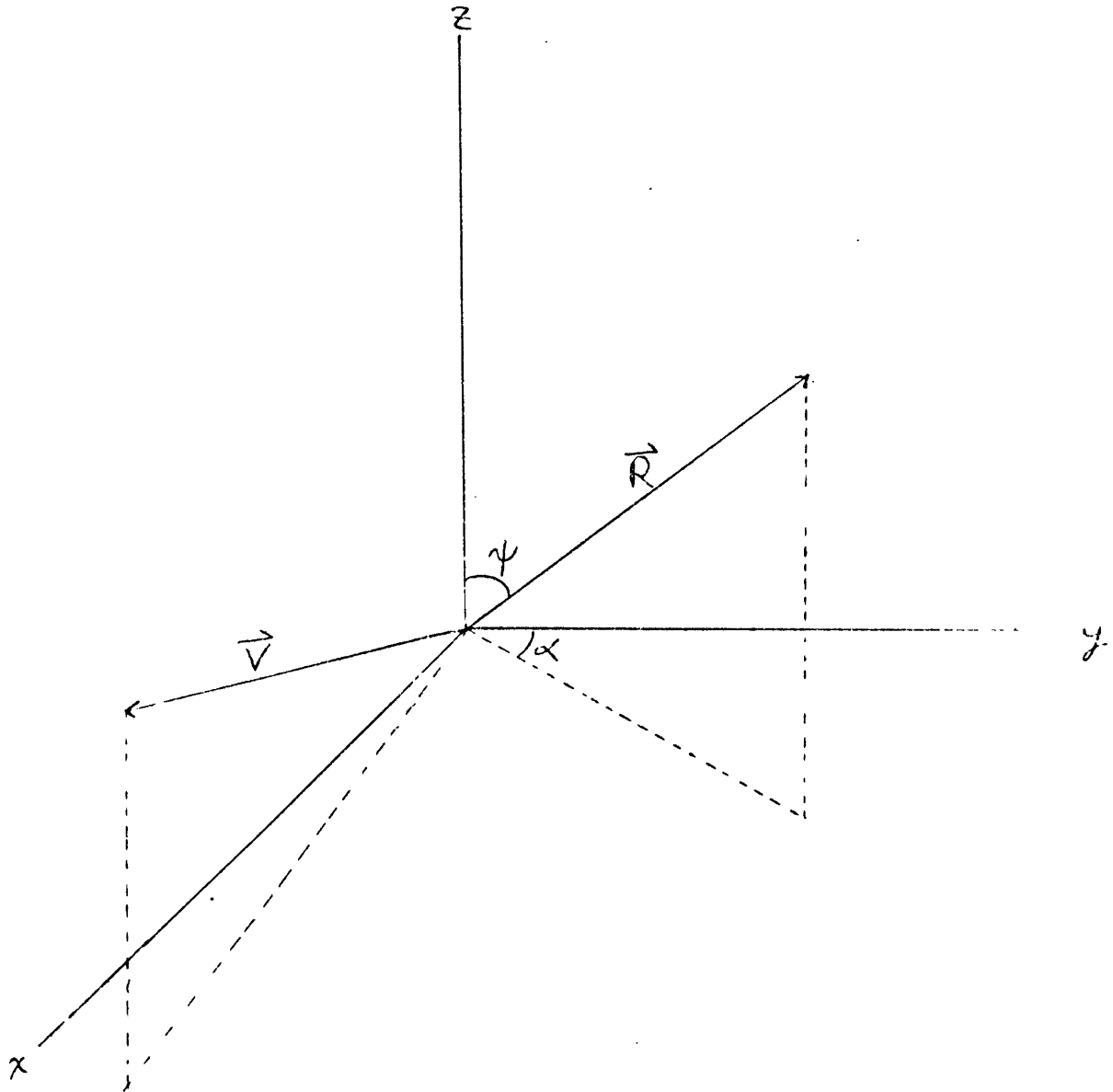


Figure 2-3

The component of the wind in the radar direction is then

$$\vec{V} \cdot \vec{R} = u \sin\psi \cos\alpha + v \sin\psi \sin\alpha + w \cos\psi .$$

For the existing "vertical" pointing, $\psi = 0.36^\circ$ and $\alpha = 50.4^\circ$, which gives

$$\begin{aligned} \vec{V} \cdot \vec{R} &= u \sin(0.36^\circ) \cos(50.4^\circ) + v \sin(0.36^\circ) \sin(50.4^\circ) + \\ &\quad w \cos(0.36^\circ) \\ &= .0040u + .0048v + 1.00w \quad . \end{aligned}$$

If we assume typical values of $u \sim v \sim 10$ m/s and $w \sim 0.1$ m/s,

$$\vec{V} \cdot \vec{R} = 4.0 + 4.8 + 10 \quad (\times 10^{-2} \text{ m/s}) .$$

This value of $\vec{V} \cdot \vec{R}$ is approximately 88% in error if used as an estimation of the vertical component of the wind. Previous calculations performed ignoring this offset are therefore considerably in error.

Another consideration in the correcting of the "vertical" beam to true vertical is the elimination of the dependence of the vertical component value on the values measured for the horizontal components. In other words, if $\psi = 0^\circ$, the equation for $\vec{V} \cdot \vec{R}$, and therefore the vertical component w , no longer depends on u and v . This is an important consideration, for it decouples the scattering volume in which the vertical component is measured from the two scattering

volumes in which horizontal wind components are measured. At stratospheric heights, these latter volumes are typically separated from the former by 1.5 km, and an assumption must be made concerning the similarity of the horizontal components in the various volumes. A truly vertical beam eliminates the need for such an assumption.

Phase Maps which correct the vertical

Method 1: Addition of cable to module pairs

Each column must have the following insertions
in units of $\lambda/4$:

4+(3 x 1.327)
4+(3 x 1.327)
4+(2 x 1.327)
4+(2 x 1.327) Phase Map IV

4+(1 x 1.327)
4+(1 x 1.327)
4
4

Method 2: Addition of cable to each successive module:

Each column must have the following insertions
in units of $\lambda/4$:

4+(3.5 x 1.259)
4+(3.0 x 1.259)
4+(2.5 x 1.259)
4+(2.0 x 1.259) Phase Map V

4+(1.5 x 1.259)
4+(1.0 x 1.259)
4+(0.5 x 1.259)
4

Method 3: Deletion of cable from each successive module:

Each column must have the following insertions
in units of $\lambda/4$:

3
3-(0.5 x 1.259)
3-(1.0 x 1.259)
3-(1.5 x 1.259) Phase Map VI

3-(2.0 x 1.259)
3-(2.5 x 1.259)
3-(3.0 x 1.259)
3-(3.5 x 1.259)

APPENDIX

Theory of Phased Arrays and Application
to the Jicamarca Radio Telescope

A radio/radar telescope such as the instrument at Jicamarca would have limited potential if the beam pattern were as fixed as the antenna. While providing an inexpensive method of constructing instruments with large collecting areas, fixed antenna design necessitates the inclusion in the design of the ability to shift the beam pattern. One manner of accomplishing this shift is to incorporate a phase gradient in the transmitters (or receivers) or transmission cables of the array.

One-Dimensional Arrays (Unphased)

In the one dimensional array, the geometry is as shown in Figure A-1. An incoming plane wave, originating at source S, is received at progressively later times at elements 1,2,3,4, and 5. The amount of phase difference seen at various elements is thus dependent on the spacing between elements, "a", the zenith angle of the source, " ψ ", and the wavelength λ . For example, the path difference r_1 between the source and element 1 and the source and element 1 and the source and element 2 is simply $a \cdot \sin\psi$. Thus the far field seen by the first two elements of the array is

$$E = E_1 + E_2 \exp[ik \cdot a \cdot \sin\psi]$$

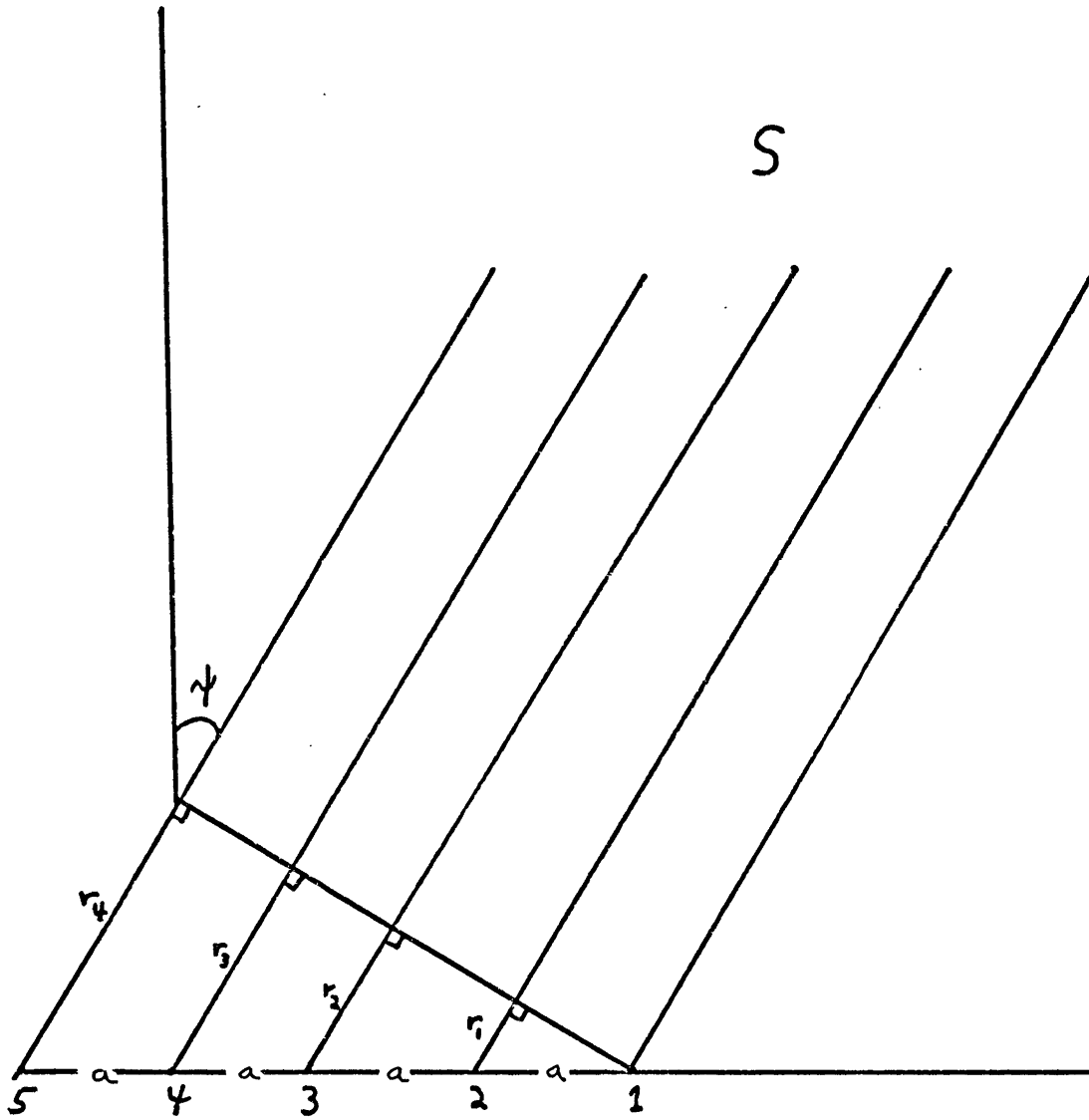


Figure A-1

where the phase reference is at element 1, and the elements are spaced by the separation a .

The path difference between element 1 and element 3 is $r_2 = 2a \cdot \sin\psi$, between 1 and 4 $r_3 = 3a \cdot \sin\psi$, and so forth. Thus the generalization of the equation given above to an "n" element array gives the far field as

$$E = E_1 + E_2 \exp[ik \cdot a \cdot \sin\psi] + E_3 \exp[ik \cdot 2a \cdot \sin\psi] + \dots + E_n \exp[ik(n-1) \cdot a \cdot \sin\psi] .$$

This may also be written as

$$E = \sum_{s=1}^n E_s e^{ik(s-1)a \cdot \sin\psi} \quad , \text{ or, assuming}$$

$$E_1 = E_2 = \dots = E_n \equiv E_0 ,$$

$$E = E_0 \sum_{s=1}^n e^{ik(s-1)a \cdot \sin\psi} .$$

It is easily shown that this may be expressed as

$$E = E_0 \frac{1 - e^{ik \cdot na \cdot \sin\psi}}{1 - e^{ik \cdot a \cdot \sin\psi}}$$

$$= E_0 \frac{1 - \cos(kna \cdot \sin\psi) - i \sin(kna \cdot \sin\psi)}{1 - \cos(ka \cdot \sin\psi) - i \sin(ka \cdot \sin\psi)} .$$

Rationalizing by squaring,

$$|E|^2 = E_0^2 \frac{[1 - \cos(kna \cdot \sin\psi) - i \sin(kna \cdot \sin\psi)]^2}{[1 - \cos(ka \cdot \sin\psi) - i \sin(ka \cdot \sin\psi)]^2}$$

$$= E_0^2 \frac{[1 - \cos(kna \cdot \sin\psi)] + \sin(kna \cdot \sin\psi)}{[1 - \cos(ka \cdot \sin\psi)] + \sin(ka \cdot \sin\psi)}$$

$$= E_0^2 \frac{1 - 2 \cos(kna \cdot \sin\psi) + 1}{1 - 2 \cos(ka \cdot \sin\psi) + 1}$$

$$= E_0^2 \frac{1 - \cos(kna \cdot \sin\psi)}{1 - \cos(ka \cdot \sin\psi)} .$$

Using the double-angle formula $\sin^2\left(\frac{\theta}{2}\right) = \frac{1 - \cos \theta}{2}$,

this becomes

$$|E|^2 = E_0^2 \frac{\sin^2\left(\frac{kna}{2} \cdot \sin\psi\right)}{\sin^2\left(\frac{ka}{2} \cdot \sin\psi\right)} .$$

In field strength, the array factor for an n-element one dimensional array of spacing "a" is therefore

$$A(\psi) = \frac{\sin\left[\frac{kna}{2} \cdot \sin\psi\right]}{\sin\left[\frac{ka}{2} \cdot \sin\psi\right]} .$$

Two-Dimensional Arrays (Unphased)

The geometry of the two-dimensional array is shown in Figure A-2. S is again a source of plane waves which arrive at various antenna elements at different times. The phase of the signal received at any element (relative, say, to element (1,1)), is a function of the path length difference between the elements and the source. The path difference between S and (1,1) and S and (v_x, v_y) is, from Figure A-2,

$$r = (v_x - 1)a_1 \sin\psi \cos\alpha + (v_y - 1)a_2 \sin\psi \sin\alpha$$

assuming parallel plane waves. Here a_1 is the element separation in the x-direction, and a_2 is the y-direction spacing.

If E_1 is the electric field amplitude at (1,1) and E_2 is the amplitude at (v_x, v_y) , the total field seen by both elements is

$$E = E_1 + E_2 e^{ik[(v_x-1)a_1 \sin\psi \cos\alpha + (v_y-1)a_2 \sin\psi \sin\alpha]} .$$

Considering an $n \times m$ array consisting of n elements in the x -direction and m elements in the y -direction, and assuming the electric field amplitude is equal at all elements, the total field seen is

$$E = E_0 \sum_{v_x=1}^n \sum_{v_y=1}^m e^{ik[(v_x-1)a_1 \sin\psi \cos\alpha + (v_y-1)a_2 \sin\psi \sin\alpha]} .$$

Proceeding as in the one-dimensional case,

$$E = E_0 \frac{1-e^{ikna_1 \sin\psi \cos\alpha}}{1-e^{ika \sin\psi \cos\alpha}} \cdot \frac{1-e^{ikna_2 \sin\psi \sin\alpha}}{1-e^{ikna \sin\psi \sin\alpha}} .$$

The array factor in power density is now

$$[A(\psi, \alpha)]^2 = \frac{\sin^2 \left[\frac{kna_1}{2} \sin\psi \cos\alpha \right]}{\sin^2 \left[\frac{ka_1}{2} \sin\psi \cos\alpha \right]} \cdot \frac{\sin^2 \left[\frac{kna_2}{2} \sin\psi \sin\alpha \right]}{\sin^2 \left[\frac{ka_2}{2} \sin\psi \sin\alpha \right]} .$$

Phased Arrays

The arrays described above have maxima normal to the arrays, since the array factors $A(\psi)$ or $A(\psi, \alpha)$ reach a maximum at $\psi = 0^\circ$. At this point, the array factors become

$$A(\psi) = n \quad (\text{one-dimensional case})$$

$$A(\psi, \alpha) = n \times m \quad (\text{two-dimensional case})$$

by L'Hospitals rule.

If the beam pattern is to be shifted in order to maximize the pattern at a zenith angle different from zero, a phase gradient must be established along the elements of the array. This may be accomplished by the inclusion of additional path lengths in the cable network feeding the array, as illustrated by the curly lines in Figure A-3.

Obviously, maximization of the beam pattern at the zenith angle of the source requires

$$r_0 + l_1 = r_1 + l_2 = r_2 + l_3 = r_3 + l_4 = \text{constant}$$

which is satisfied if

$$l_1 = r_3 \quad l_2 = r_3 - r_1 \quad l_3 = r_3 - r_2 \quad l_4 = r_0 (=0).$$

In this manner, a signal originating at zenith angle ψ traverses identical path lengths to all four receivers, thus equalizing the phase and maximizing the observed field.

The additional cables make the total field seen by a two-element array with spacing "a" and cable insertion " ℓ " equal to

$$E = E_1 + E_2 \exp[ik(a \cdot \sin \psi - \ell)]$$

where ψ , as before, is the zenith angle of the source, and

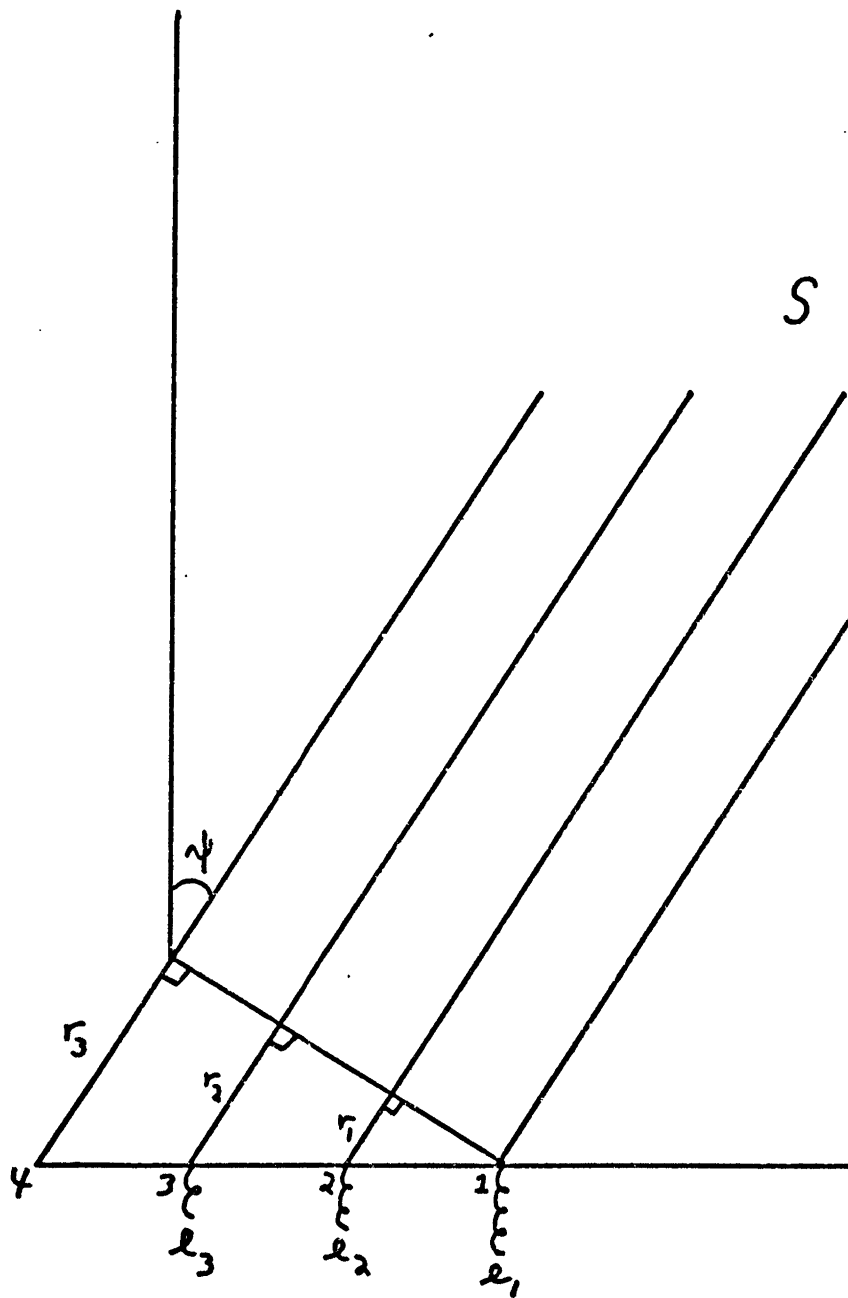


Figure A-3

the phase reference is the farthest element from the source.

Similarly, if an additional cable of length ℓ , 2ℓ , 3ℓ , etc. is attached to each successive element of an n -element array, the field seen is

$$E = E_1 + E_2 \exp[ik(a \cdot \sin\psi - \ell)] + E_3 \exp[ik(2a \cdot \sin\psi - 2\ell)] + \\ E_4 \exp[ik(3a \cdot \sin\psi - 3\ell)] + \dots + E_n \exp[ik(n-1)(a \cdot \sin\psi - \ell)] .$$

As before, this may be written

$$E = \sum_{s=1}^n E_s e^{ik(s-1)(a \cdot \sin\psi - \ell)} .$$

A calculation similar to that in the unphased case yields the array factor

$$A(\psi) = \frac{\sin[\frac{kna}{2} \sin\psi - \frac{kn}{2} \ell]}{\sin[\frac{ka}{2} \sin\psi - \frac{k\ell}{2}]} .$$

This expression is easily extended to the two-dimensional array. Assuming n elements in the x -direction, spaced by amount a_1 , and with progressive cable insertions of length ℓ_1 , and m elements spaced by a_2 and with cable insertions of length ℓ_2 in the y -direction, the far field seen at the receivers is

$$E = E_0 \sum_{v_x=1}^n \sum_{v_y=1}^m e^{ik[(v_x-2)(a_1 \sin\psi \cos\alpha - \ell_1) + (v_y-1)(a_2 \sin\psi \sin\alpha - \ell_2)]} .$$

Thus the array factor is

$$A(\psi, \alpha) = \frac{\sin[n\frac{k}{2}a_1 \sin\psi \cos\alpha - n\frac{k}{2}\ell_1]}{\sin[\frac{k}{2}a_1 \sin\psi \cos\alpha - \frac{k}{2}\ell_1]} \cdot \frac{\sin[m\frac{k}{2}a_2 \sin\psi \sin\alpha - m\frac{k}{2}\ell_2]}{\sin[\frac{k}{2}a_2 \sin\psi \sin\alpha - \frac{k}{2}\ell_2]} .$$

This is the array factor for a two-dimensional array (Kraus, 1950 and Jasik , 1961), but its validity requires 3 assumptions:

1. Along either axis of the array, the spacing a_1 (or a_2) between elements remains constant.
2. Along either axis the additional cable insertions l_1 (or l_2) between elements remain constant.
3. The source is far enough away to insure plane waves.

The first two assumptions are tantamount to the approximation of a "uniform phase gradient" across the array, i.e., the phase difference between any two elements is equal to the phase difference between any other consecutive elements (Wolff, 1966).

This expression neglects, then, two features of the actual instrument at Jicamarca, namely, an extra $\frac{\lambda}{2}$ in separation between quarters of the array, and, more importantly, the fact that clusters of 144 dipoles form each module, and no phasing is inserted between dipoles of a given module. These characteristics have been neglected in previous calculation (Ochs, 1965 and Rastogi, 1975) which simply applied the expression derived above for a uniform phase gradient array. Calculations of this kind will be illustrated first, followed by the calculation which accounts for the particularities of the telescope at Jicamarca.

An explicit determination of the array factor as applied at Jicamarca, even in the simplified calculation, requires

some knowledge of the characteristics of the antenna. In the "uniform phase gradient" approximation, the following values will be (and have been) used:

Wavelength: $\lambda = 6\text{m}$

Spacing Between Elements: $a_1 = a_2 = \lambda/2$

Wavenumber: $k = 2\pi/\lambda = 2\pi/6\text{m}$

Number of Elements Along Axis: $n = m = 96$.

The remaining parameter necessary for the evaluation of the array factor, the length of cable insertions, is provided by a "phase map", of which the following is an example:

N_m (1960)	E_m	
3333	3333	
3333	3333	
2222	2222	
2222	2222	
		Phase Map I
5555	5555	
5555	5555	
4444	4444	
4444	4444	
W_m	S_m	

The map is interpreted as follows: each number represents a cable insertion to one module, which consists of 144 cophased dipoles. The number is the length, in quarter wavelengths, of the insertion. Thus "4" represents 4 quarter wavelengths, or one full wavelength of cable inserted. Similarly, "3" refers to $.75\lambda$ inserted, "2" = $.5\lambda$, and "5" (the equivalent of "1") means 1.25λ inserted. Obviously, a factor of 4 may be added or subtracted from the maps at random, since a pathlength difference of an integral number of wavelengths has no effect on the phase

of the signal seen by various elements. The usage of "4" and "5" rather than "0" and "1" stems only from physical considerations and availability of insertions of lengths of .5, .75, 1.0, and 1.25 wavelengths.

The uniform phase gradient calculation, as applied to the dipoles of the antenna, dictates an even division of the phase change among the dipoles in a line. Thus if a total change across the antenna of 1 wavelength is evenly divided among 96 dipoles, the result is an equivalent cable insertion at each dipole of $\lambda/96$ along the x-axis. As shown by the map, there is no phase gradient in the y-direction, making $\ell_2 = 0$. The two-dimensional array factor is now

$$A(\psi, \alpha) = \frac{\sin[96 \cdot \frac{\pi}{\lambda} \cdot \frac{\lambda}{2} \sin\psi \cos\alpha - 96 \cdot \frac{\pi}{\lambda} \cdot \frac{\lambda}{96}]}{\sin[\frac{\pi}{\lambda} \cdot \frac{\lambda}{2} \sin\psi \cos\alpha - \frac{\pi}{\lambda} \cdot \frac{\lambda}{96}]}$$

$$\cdot \frac{\sin[96 \cdot \frac{\pi}{\lambda} \cdot \frac{\lambda}{2} \sin\psi \sin\alpha]}{\sin[\frac{\pi}{\lambda} \cdot \frac{\lambda}{2} \sin\psi \sin\alpha]}$$

or

$$A(\psi, \alpha) = \frac{\sin[48\pi \sin\psi \cos\alpha - \pi]}{\sin[\frac{\pi}{2} \sin\psi \cos\alpha - \frac{\pi}{96}]} \cdot \frac{\sin[48\pi \sin\psi \sin\alpha]}{\sin[\frac{\pi}{2} \sin\psi \sin\alpha]}$$

The beam pattern resulting from such a factor may be discerned by considering the behavior of $A(\psi, \alpha)$ for $\alpha = 0.0^\circ$ (i.e., along the NE-SW axis). This gives

$$A(\psi, 0) = \frac{\sin[48\pi \sin\psi - \pi]}{\sin[\frac{\pi}{2} \sin\psi - \frac{\pi}{96}]}$$

This exhibits the well-known behavior of $\frac{\sin nx}{\sin x}$, that is, a maximum occurs whenever the numerator maximizes, or when both numerator and denominator are zero, while a minimum occurs when only the numerator approaches zero. Thus in the above case a maximum occurs when

$$\begin{aligned} 48\pi \sin\psi - \pi &= 0 \\ \sin \psi &= 1/48 \\ \psi &= 1.19^\circ . \end{aligned}$$

This is the position of the first maximum, and corresponds to the offset of the beam from the direction perpendicular to the array. The first minima occur at

$$\begin{aligned} 48\pi \sin\psi - \pi &= -\pi \\ \sin \psi &= 0 \\ \psi &= 0.0^\circ \end{aligned}$$

and

$$\begin{aligned} 48\pi \sin\psi - \pi &= \pi \\ \sin \psi &= 1/24 \\ \psi &= 2.39^\circ . \end{aligned}$$

The positions of the secondary maxima corresponding to the first side lobes are equally spaced in $\sin\psi$, and occur at $\psi = 2.98^\circ$ and $\psi = -0.59^\circ$. These lobes are 27dB below the main beam. A plot of $A(\psi, \alpha)$ for this case is given in Figure A-4.

The preceding calculations, based upon the "uniform phase gradient" assumption, are inaccurate when applied to the instrument at Jicamarca for the two reasons mentioned above:

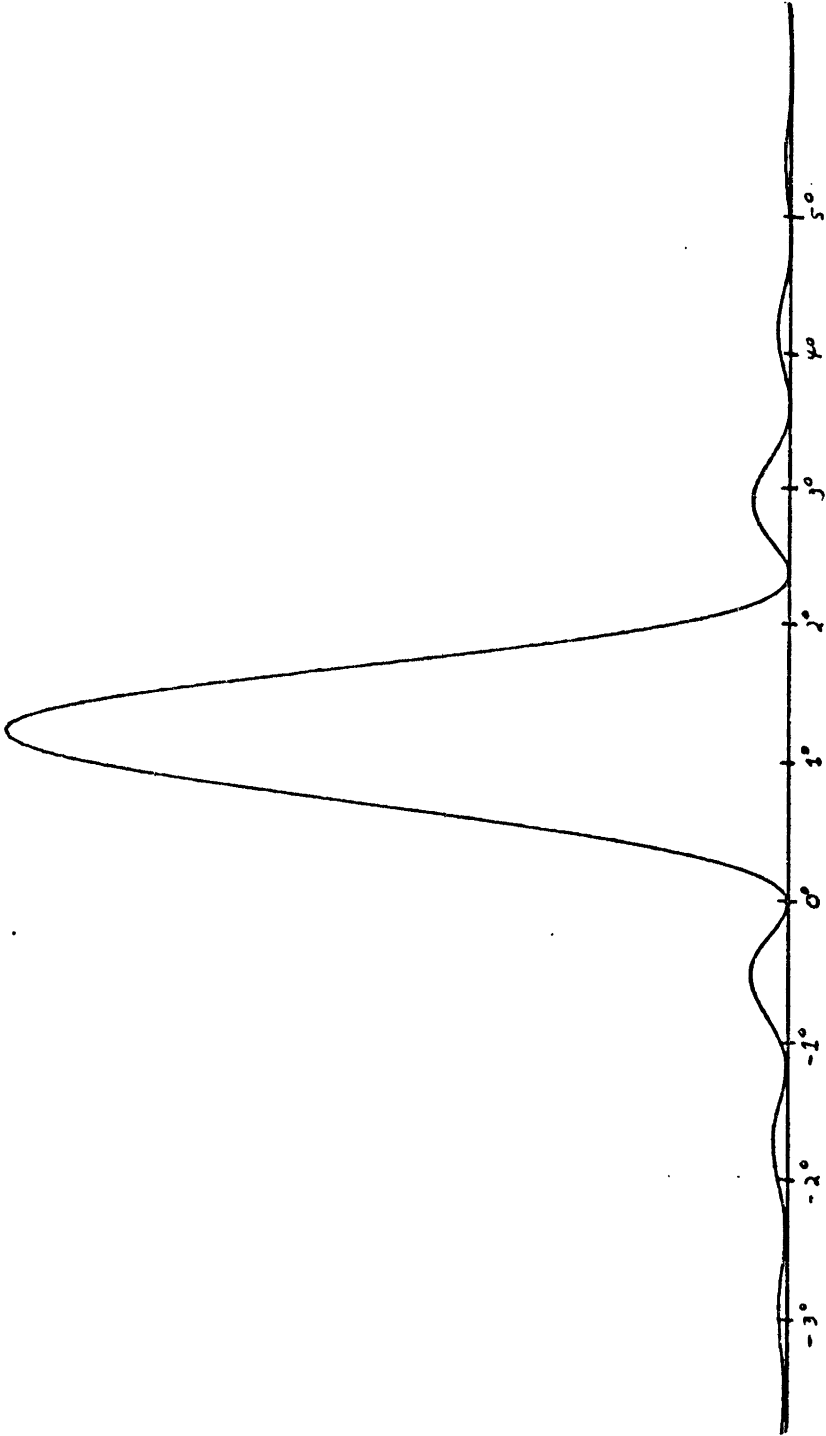


Figure A-4

1. Within each module, the 12 dipoles along either axis are cophased, i.e., have equal length feed cables.
2. The spacing between modules is not uniform, due to the presence of a $\lambda/2$ gap between quarters.

For these reasons, the array factor for the Jicamarca antenna is more complex than $A(\psi, \alpha)$ as calculated above, and is in fact the product of three such factors. They are:

- A_1 - A factor representing 144 dipoles, separated by $\lambda/2$ and cophased. These 144 dipoles make up one module.
- A_2 - A factor representing 16 modules, phased with cable insertions of lengths l_{ij} and separated by 6λ . These 16 modules make up one quarter.
- A_3 - A factor representing 4 quarters, phased by module cable insertion or directly at the switchyard, and separated by 24.5λ .

A schematic view of the antenna illustrating the groups of elements just described is given in Figure A-5.

The rationale for the grouping as depicted in Figure A-5 is simple. Within each group, the requirements of the "uniform phase gradient" assumption are satisfied. For example, within each module, the dipoles are separated by uniform distance and phased by cable insertions of a constant length (0 in this case). Within each quarter, the modules are also equidistant and phased with a uniform gradient. And, within the entire antenna, the quarters also satisfy

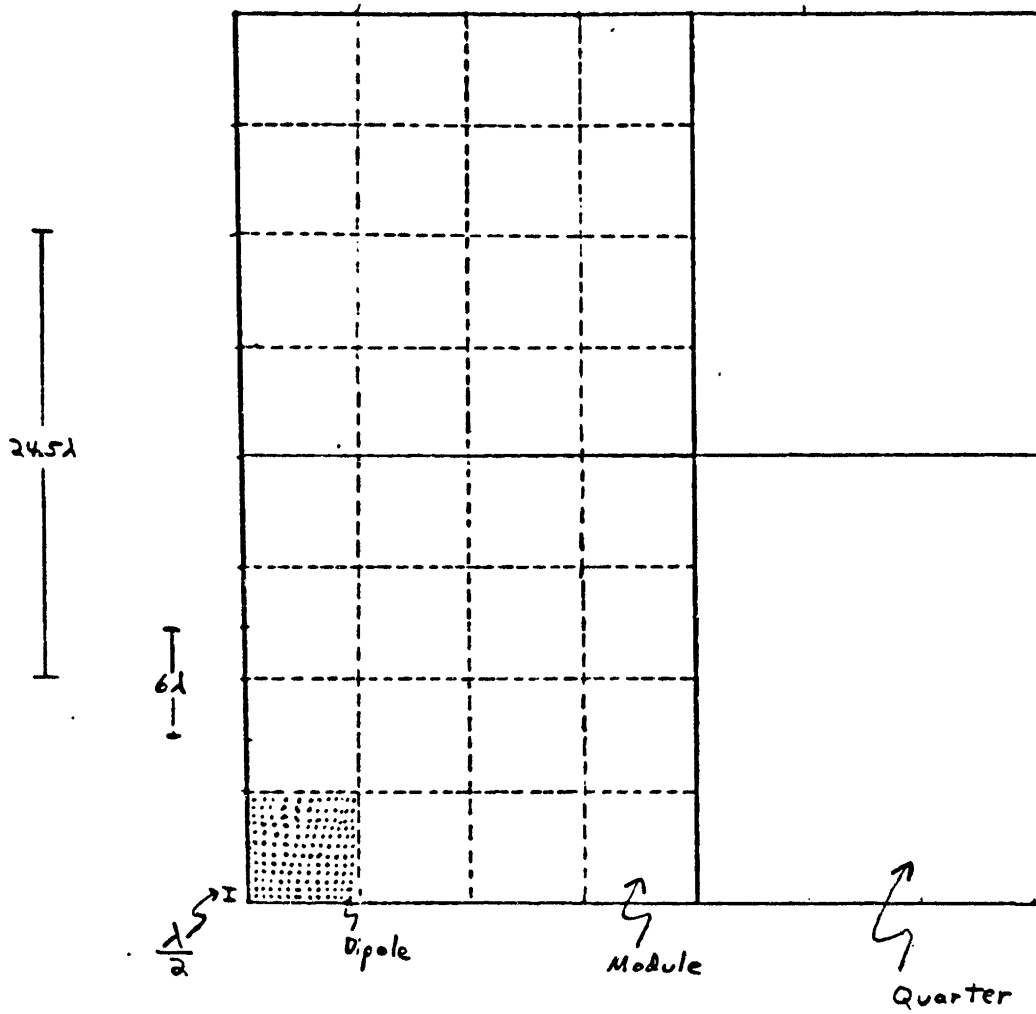


Figure A-5

these requirements. The full array factor for the Jicamarca antenna is therefore

$$\begin{aligned}
 A_T(\psi, \alpha) &= A_1(\psi, \alpha) \cdot A_2(\psi, \alpha) \cdot A_3(\psi, \alpha) \\
 &= \frac{\sin\left[n \frac{k}{D^2} a_D \sin\psi \cos\alpha - n \frac{k}{D^2} \ell_{1D}\right]}{\sin\left[\frac{k}{2} a_{1D} \sin\psi \cos\alpha - \frac{k}{2} \ell_{1D}\right]} \cdot \frac{\sin\left[m \frac{k}{D^2} a_{2D} \sin\psi \sin\alpha - m \frac{k}{D^2} \ell_{2D}\right]}{\sin\left[\frac{k}{2} a_{2D} \sin\psi \sin\alpha - \frac{k}{2} \ell_{2D}\right]} \\
 &\times \frac{\sin\left[n \frac{k}{M^2} a_{1M} \sin\psi \cos\alpha - n \frac{k}{M^2} \ell_{1M}\right]}{\sin\left[\frac{k}{2} a_{1M} \sin\psi \cos\alpha - \frac{k}{2} \ell_{1M}\right]} \cdot \frac{\sin\left[m \frac{k}{M^2} a_{2M} \sin\psi \sin\alpha - m \frac{k}{M^2} \ell_{2M}\right]}{\sin\left[\frac{k}{2} a_{2M} \sin\psi \sin\alpha - \frac{k}{2} \ell_{2M}\right]} \\
 &\times \frac{\sin\left[n \frac{k}{Q^2} a_{1Q} \sin\psi \cos\alpha - n \frac{k}{Q^2} \ell_{1Q}\right]}{\sin\left[\frac{k}{2} a_{1Q} \sin\psi \cos\alpha - \frac{k}{2} \ell_{1Q}\right]} \cdot \frac{\sin\left[m \frac{k}{Q^2} a_{2Q} \sin\psi \sin\alpha - m \frac{k}{Q^2} \ell_{2Q}\right]}{\sin\left[\frac{k}{2} a_{2Q} \sin\psi \sin\alpha - \frac{k}{2} \ell_{2Q}\right]}
 \end{aligned}$$

where

$$\begin{aligned}
 \frac{n_D}{\binom{M}{Q}} &= \text{numbers of } \left\{ \begin{array}{l} \text{dipoles} \\ \text{modules} \end{array} \right\} \text{ in x-direction per } \left\{ \begin{array}{l} \text{modules} \\ \text{quarters} \end{array} \right\} \text{ antenna} \\
 \frac{m_D}{\binom{M}{Q}} &= \text{ " " " " y-direction " " } \\
 \frac{a_{1D}}{\binom{M}{Q}} &= \text{spacing of } \left\{ \begin{array}{l} \text{dipoles} \\ \text{modules} \end{array} \right\} \text{ in x-direction} \\
 &\quad \text{quarters} \\
 \frac{a_{2D}}{\binom{M}{Q}} &= \text{ " " " " y-direction} \\
 \frac{\ell_{1D}}{\binom{M}{Q}} &= \text{cable insertions between } \left\{ \begin{array}{l} \text{dipoles} \\ \text{modules} \end{array} \right\} \text{ in x-direction} \\
 &\quad \text{quarters} \\
 \frac{\ell_{2D}}{\binom{M}{Q}} &= \text{ " " " " y-direction}
 \end{aligned}$$

Inserting the values pertinent to Jicamarca, the complete array factor becomes

$$\begin{aligned}
A_T(\psi, \alpha) &= \frac{\sin[6\pi\sin\psi\cos\alpha]}{\sin[\frac{\pi}{2}\sin\psi\cos\alpha]} \cdot \frac{\sin[6\pi\sin\psi\sin\alpha]}{\sin[\frac{\pi}{2}\sin\psi\sin\alpha]} \\
&\times \frac{\sin[24\pi\sin\psi\cos\alpha - 4\frac{\pi}{\lambda}l_{1M}]}{\sin[6\pi\sin\psi\cos\alpha - \frac{\pi}{\lambda}l_{1M}]} \cdot \frac{\sin[24\pi\sin\psi\sin\alpha - 4\frac{\pi}{\lambda}l_{2M}]}{\sin[6\pi\sin\psi\sin\alpha - \frac{\pi}{\lambda}l_{2M}]} \\
&\times \frac{\sin[49\pi\sin\psi\cos\alpha - 2\frac{\pi}{\lambda}l_{1Q}]}{\sin[\frac{49}{2}\pi\sin\psi\cos\alpha - \frac{\pi}{\lambda}l_{1Q}]} \cdot \frac{\sin[49\pi\sin\psi\sin\alpha - 2\frac{\pi}{\lambda}l_{2Q}]}{\sin[\frac{49}{2}\pi\sin\psi\sin\alpha - \frac{\pi}{\lambda}l_{2Q}]}
\end{aligned}$$

A.1

All that remains undetermined in this expression (aside, naturally, from ψ and α) are the lengths of the cable insertions l_{1M} , l_{2M} , l_{1Q} , and l_{2Q} . Once these have been specified, the beam pattern of the antenna may be determined at all points by evaluating $A_T(\psi, \alpha)$.

However, in certain cases, including the current "vertical" phasing as shown in Phase Map I, the phasing cables may be inserted in such a manner as to alter slightly the expression derived above. It will be noted that the "uniform phase gradient" assumption is not applicable to the modules as phased in this case, since, along the NE-SW_m axis, equal cable lengths are inserted in each successive pair of modules rather than each module. However, the expression derived for $A_T(\psi, \alpha)$ may be salvaged if the first term, formerly representing 144 cophased dipoles (12 along each axis) is expanded to include 576 cophased dipoles (24 per axis). Furthermore, the second term, instead of representing the 16 modules in a quarter,

is made to account for the four "module pairs" now existing per quarter. Insertion of the values $\ell_{1M} = \lambda/4$, $\ell_{2M} = 0$, $\ell_{1Q} = \lambda/2$, and $\ell_{2Q} = 0$ used in the "vertical" phase scheme, the expression for $A_T(\psi, \alpha)$ becomes

$$A_T(\psi, \alpha) = \frac{\sin[12\pi\sin\psi\cos\alpha]}{\sin[\frac{\pi}{2}\sin\psi\cos\alpha]} \cdot \frac{\sin[12\pi\sin\psi\sin\alpha]}{\sin[\frac{\pi}{2}\sin\psi\sin\alpha]}$$

$$\times \frac{\sin[24\pi\sin\psi\cos\alpha - \frac{\pi}{2}]}{\sin[12\pi\sin\psi\cos\alpha - \frac{\pi}{2}]} \cdot \frac{\sin[24\pi\sin\psi\sin\alpha]}{\sin[12\pi\sin\psi\sin\alpha]}$$

$$\times \frac{\sin[49\pi\sin\psi\cos\alpha - \pi]}{\sin[\frac{49}{2}\pi\sin\psi\cos\alpha - \frac{\pi}{2}]} \cdot \frac{\sin[49\pi\sin\psi\sin\alpha]}{\sin[\frac{49}{2}\pi\sin\psi\sin\alpha]}$$

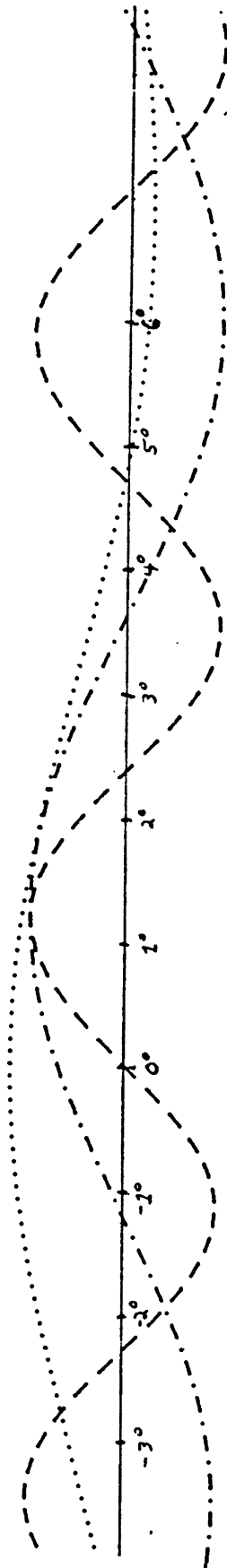
It is the product of these "subfactors" representing A_1 , A_2 , and A_3 which determines the beam pattern of the array. Suppression, distortion, or enhancement of various side lobes may result from the combination of these subfactors. This is most easily seen by considering, again, the behavior of each subfactor, as well as their product $A_T(\psi, \alpha)$ along the NE-SW_m axis ($\alpha=0$). Then

$$A_1 \propto \frac{\sin[12\pi\sin\psi]}{\sin[\frac{\pi}{2}\sin\psi]}$$

$$A_2 \propto \frac{\sin[24\pi\sin\psi - \frac{\pi}{2}]}{\sin[12\pi\sin\psi - \frac{\pi}{4}]}$$

$$A_3 \propto \frac{\sin[49\pi\sin\psi - \pi]}{\sin[\frac{49}{2}\pi\sin\psi - \frac{\pi}{2}]}$$

Each of these subfactors is displayed in Figure A-6 for the range $\psi = -4.0^\circ$ to $\psi = +8.0^\circ$. The reader is cautioned



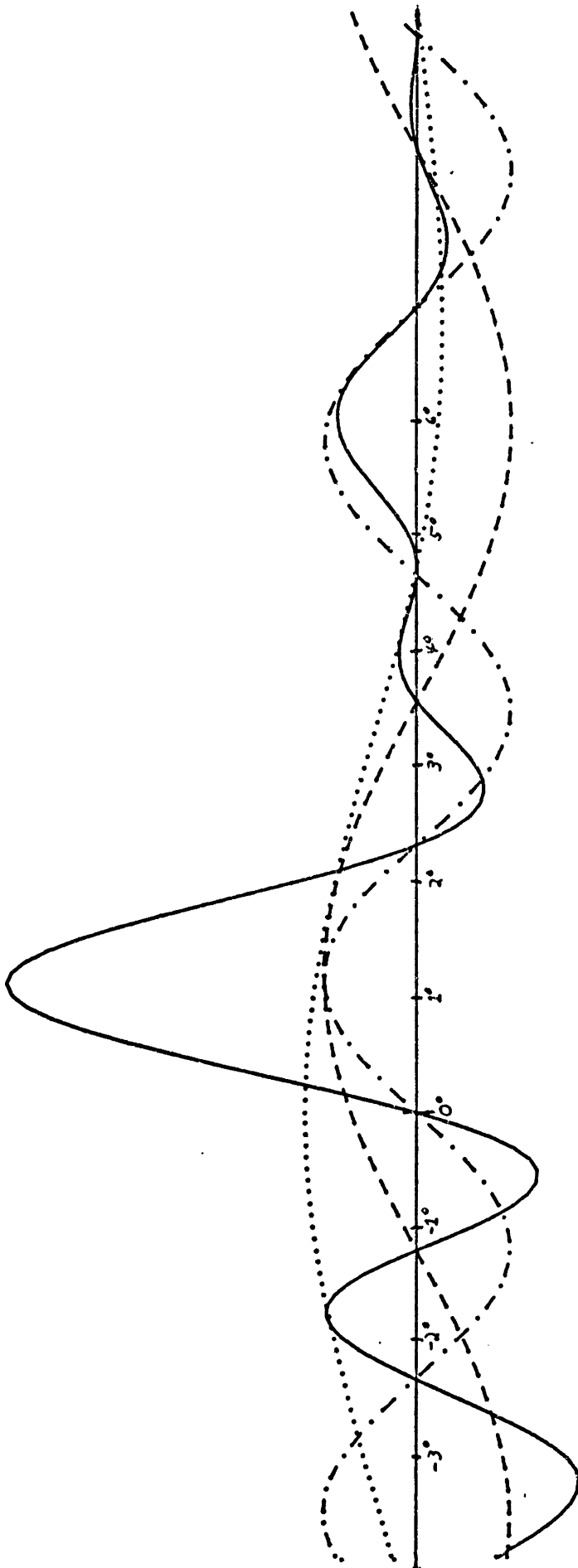
A_1
 A_2 - · - · - ·
 A_3 - - -

Figure A-6

against drawing conclusions from the relative sizes of the subfactors, since the scaling factor in the plotting routine changes between subfactors. Naturally, within A_1 , A_2 , or A_3 , the relative sizes of maxima and minima are significant, since the scaling factor is constant within each such subfactor.

One of the more obvious, and more important aspects of Figure A-6 concerns subfactor A_1 which represents one module pair of cophased dipoles. Since the elements within this group are cophased, the array subfactor maximizes directly overhead at $\psi = 0^\circ$, as opposed to A_2 and A_3 which maximize at $\psi > 1^\circ$. Also important is the position of the maximum of subfactor A_3 , which occurs at 1.17° , 0.02° away from the maximum of A_2 at 1.19° . This coincides with that computed using the "uniform phase gradient" assumption applied to the dipoles.

The effect of the various locations of subfactor maxima may be seen in Figure A-7, which shows the product A_T as well as the subfactors A_1 , A_2 , and A_3 . The maximum value of A_T occurs at 1.10° , nearly one-tenth of a degree removed from the value predicted by the simplified calculation. As indicated by Figure A-7, the effect of the array subfactor representing the clusters of cophased dipoles is to displace the main lobe maximum toward the overhead direction ($\psi = 0^\circ$). The array subfactor for the quarters, while maximizing nearer 0° than that of the module pairs, serves to lessen the effect of the A_1 subfactor.



A_1
 A_2 - - - -
 A_3 - · - · -
 A_4 ———

Figure A-7

Figure A-8 displays the array factor for the "vertical" beam in terms of power density rather than electric field, making the side lobes more apparent. The first side lobe beyond the main lobe (from the origin) is 21 dB below the main beam, which is lower than expected from the simplified calculation. The first side lobe on the origin side of the main beam is 31 dB below the main lobe.

In this manner, beam patterns may be calculated for the Jicamarca antenna in a variety of configurations. Those utilizing the full antenna simply employ expression A.1 with relevant values of cable lengths inserted. Two examples of this are the "West" and "South"-looking phase schemes represented by the phase maps

N_m	E_m	N_m	E_m
5432	5432	2345	2345
5432	5432	2345	2345
2543	2543	3452	3452
2543	2543	3452	3452
3254	3254	4523	4523
3254	3254	4523	4523
4325	4325	5234	5234
4325	4325	5234	5234
W_m	S_m	W_m	S_m
Phase Map II		Phase Map III	

Expression A.1 may be used to find the beam patterns for these cable insertions, provided correct values for the number of elements and spacing along each axis are utilized. For example, the first configuration requires

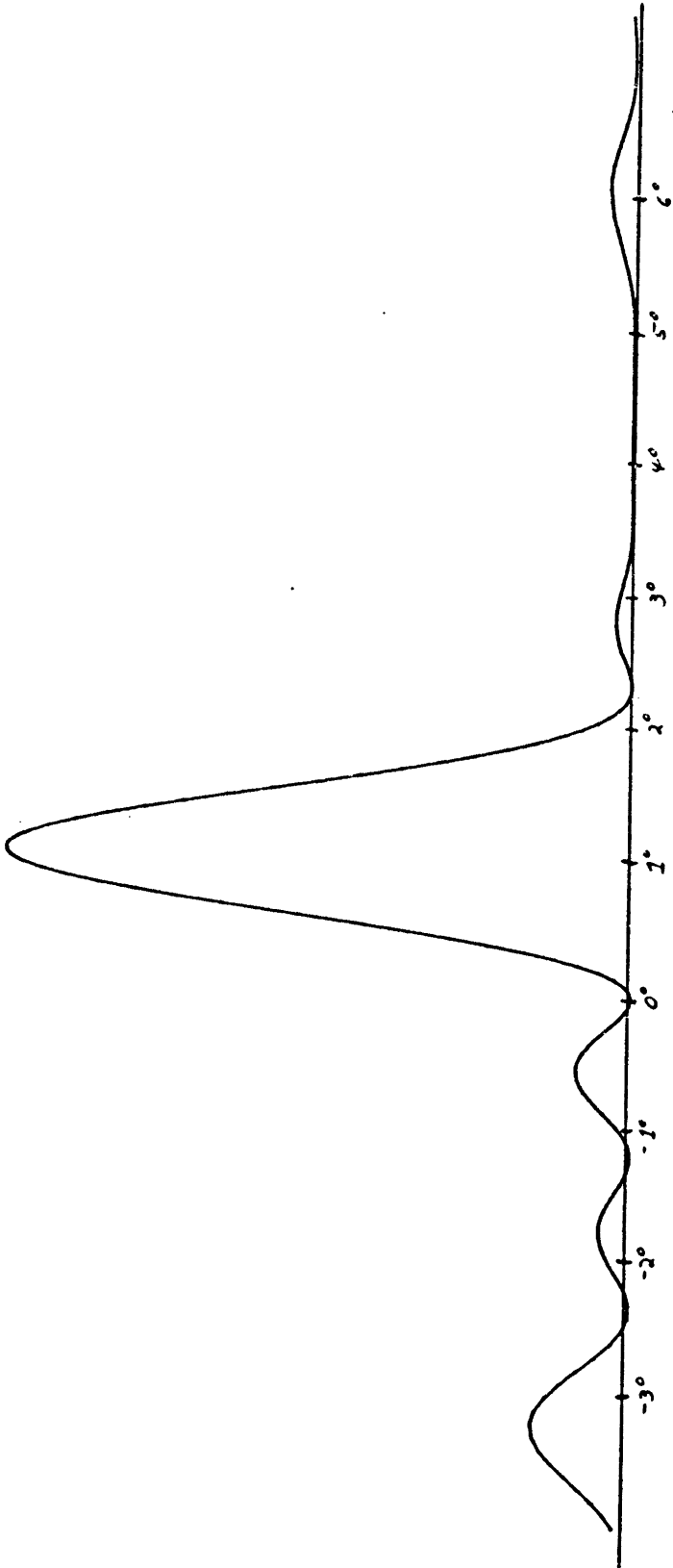


Figure A-8

$$\begin{array}{llll}
a_{1D} = \lambda/2 & a_{2D} = \lambda/2 & n_D = 24 & m_D = 12 \\
a_{1M} = 12\lambda & a_{2M} = 6\lambda & n_M = 2 & m_M = 4 \\
a_{1Q} = 24.5\lambda & a_{2Q} = 24.5\lambda & n_Q = 2 & m_Q = 2 \\
\ell_{1n} = -\lambda/4 & \ell_{2n} = \lambda/4 & & \\
\ell_{1Q} = -\lambda/2 & \ell_{2Q} = \lambda & &
\end{array}$$

The expression for $A_T(\psi, \alpha)$ is now

$$\begin{aligned}
A_T(\psi, \alpha) &= \frac{\sin[12\pi\sin\psi\cos\alpha]}{\sin[\frac{\pi}{2}\sin\psi\cos\alpha]} \dots \frac{\sin[6\pi\sin\psi\sin\alpha]}{\sin[\frac{\pi}{2}\sin\psi\sin\alpha]} \\
&\times \frac{\sin[24\pi\sin\psi\cos\alpha + \frac{\pi}{2}]}{\sin[12\pi\sin\psi\cos\alpha + \frac{\pi}{4}]} \cdot \frac{\sin[24\pi\sin\psi\sin\alpha - \pi]}{\sin[12\pi\sin\psi\sin\alpha - \frac{\pi}{2}]} \\
&\times \frac{\sin[49\pi\sin\psi\cos\alpha + \pi]}{\sin[\frac{49}{2}\pi\sin\psi\cos\alpha + \frac{\pi}{2}]} \cdot \frac{\sin[49\pi\sin\psi\sin\alpha - 2\pi]}{\sin[\frac{49}{2}\pi\sin\psi\sin\alpha - \pi]}
\end{aligned}$$

This is somewhat more complex than previous expressions and substantial computation is required to reveal the beam pattern in two dimensions. The results indicate the beam moves 1.10° along the magnetic SW-axis, and 2.31° along the magnetic NW-axis. The new position, along with the position of the "South"-looking beam are shown in Figure 2.2.

Partial Antenna Patterns

The patterns computed above result when the entire antenna is utilized with various cable insertions. In practice, however, one or two quarters of the antenna may be used for one purpose, and the remaining sections for another. For example, the north and west quarters may be phased so as to achieve the "West" pointing while the south and east quarters look toward the South. In this way, simultaneous measurement of different horizontal wind components may be accomplished.

Naturally, the patterns will be somewhat altered from those using the full antenna, depending upon which configuration is used. Three possible combinations are considered.

1. One Quarter

In this case, one quarter of the antenna is pointed in some direction, independent of the other three quarters. The effect is simply the removal of subfactor A_3 , the "quarter" subfactor, leaving the total array factor

$$A_T(\psi, \alpha) = A_1(\psi, \alpha) \cdot A_2(\psi, \alpha)$$

or

$$A_T(\psi, \alpha) = \frac{\sin[6\pi\sin\psi\cos\alpha]}{\sin[\frac{\pi}{2}\sin\psi\cos\alpha]} \cdot \frac{\sin[6\pi\sin\psi\sin\alpha]}{\sin[\frac{\pi}{2}\sin\psi\sin\alpha]}$$

$$\times \frac{\sin[24\pi\sin\psi\cos\alpha - 4\frac{\pi}{\lambda}l_{1n}]}{\sin[6\pi\sin\psi\cos\alpha - \frac{\pi}{\lambda}l_{1n}]} \cdot \frac{\sin[24\pi\sin\psi\sin\alpha - 4\frac{\pi}{\lambda}l_{2n}]}{\sin[6\pi\sin\psi\sin\alpha - \frac{\pi}{\lambda}l_{2n}]}$$

which is expression A.1 with $n = m = 1$.

The effect of the deletion of the third subfactor is dependent upon the phasing being used. For an example, the west-looking configuration, previously found to move the beam 2.31° and 1.10° along the magnetic NW and SW axes, respectively, now requires an array factor

$$A_T(\psi, \alpha) \frac{\sin[12\pi\sin\psi\cos\alpha]}{\sin[\frac{\pi}{2}\sin\psi\cos\alpha]} \cdot \frac{\sin[6\pi\sin\psi\sin\alpha]}{\sin[\frac{\pi}{2}\sin\psi\sin\alpha]}$$

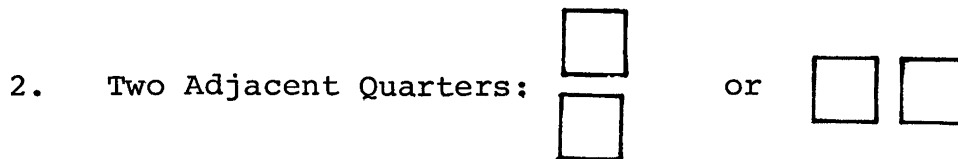
$$\times \frac{\sin[24\pi\sin\psi\cos\alpha + \frac{\pi}{2}]}{\sin[12\pi\sin\psi\cos\alpha + \frac{\pi}{4}]} \cdot \frac{\sin[24\pi\sin\psi\sin\alpha - \pi]}{\sin[6\pi\sin\psi\sin\alpha - \frac{\pi}{4}]}$$

which moves the beam only 2.24° NW and 0.89° SW_m. It is apparent that the tendency of the groups of cophased dipoles to look directly overhead has a greater effect in the absence of the "quarter" subfactor.

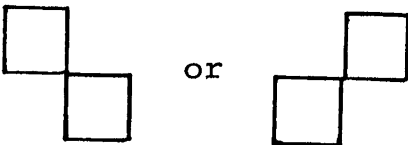
A further effect, a consequence of reducing the aperture, is the increasing of the beamwidth. The half-power beamwidth for a rectangular aperture may be shown to be (Kraus, 1966)

$$\alpha \approx \frac{50.7^\circ}{A_\lambda}$$

where A_λ is the linear dimension of the array in units of λ . Thus halving A_λ serves to double the half-power width of the beam. The Jicamarca beam, ordinarily 1.06° , is therefore 2.12° when one quarter is utilized.



An array composed of two adjacent quarters is most easily understood as a combination of the "one quarter only" case along one axis and the "full antenna" case along the other. As expected, the beam shift along the axis on which the quarters lie is identical to that accomplished by the full antenna for the same axis. The beam shift along the axis perpendicular to that along which the quarters lie is that of one quarter. Expression A.1 is readily adaptable to this case, provided the correct values for n_Q and m_Q are used (either $n_Q = 1, m_Q = 2$, or $n_Q = 2, m_Q = 1$). The shape of the beam in this case becomes elliptical, since the aperture along one axis is twice that of the other. The beamwidth along the major axis is 1.06° , along the minor axis 2.12° . Antenna Beam Maps 4 and 5 display array factor amplitudes for the main and side lobes of the two possible "adjacent quarter" divisions of the antenna. Division along a NE_m-SW_m axis is clearly preferable in terms of relative side lobe amplitudes.

3. Diagonal Quarters:  or

The expression derived for the full antenna array factor must be modified more seriously for this configuration. Clearly, the summing process in the equation

$$E_T = E_0 \sum_{v_x=1}^n \sum_{v_y=1}^n \exp\{ik[(v_x-1)(a_1 \sin\psi \cos\alpha - l_1) + (v_y-1)a_2 \sin\psi \sin\alpha - l_2]\}$$

must be carried out in a very special way, retaining only the terms corresponding to the two desired quarters. The "quarter" subfactor is then

$$A_3(\psi, \alpha) = \frac{\sin[N_Q \frac{k}{2}(a_{1Q} \sin\psi \cos\alpha + a_{2Q} \sin\psi \sin\alpha - l_{1Q} - l_{2Q})]}{\sin[\frac{k}{2}(a_{1Q} \sin\psi \cos\alpha + a_{2Q} \sin\psi \sin\alpha - l_{1Q} - l_{2Q})]}$$

where all variables are identical to those defined in the full antenna case, with the addition of " N_Q " — representing the number of elements along the diagonal line. N_Q is always 2 for the Jicamarca antenna, making the complete array factor for the bow-tie geometry

$$A_T(\psi, \alpha) = \frac{\sin[6\pi \sin\psi \cos\alpha]}{\sin[\frac{\pi}{2} \sin\psi \cos\alpha]} \cdot \frac{\sin[6\pi \sin\psi \sin\alpha]}{\sin[\frac{\pi}{2} \sin\psi \sin\alpha]}$$

$$\times \frac{\sin[24\pi \sin\psi \cos\alpha - 4\frac{\pi}{\lambda} l_{1n}]}{\sin[6\pi \sin\psi \cos\alpha - \frac{\pi}{\lambda} l_{1n}]} \cdot \frac{\sin[24\pi \sin\psi \sin\alpha - 4\frac{\pi}{\lambda} l_{2n}]}{\sin[6\pi \sin\psi \sin\alpha - \frac{\pi}{\lambda} l_{2n}]}$$

$$\times \frac{\sin[49\pi(\sin\psi \cos\alpha + \sin\psi \sin\alpha) - \frac{2\pi}{\lambda}(l_{1Q} + l_{2Q})]}{\sin[\frac{49}{2}\pi(\sin\psi \cos\alpha + \sin\psi \sin\alpha) - \frac{\pi}{\lambda}(l_{1Q} + l_{2Q})]}$$

• 707
(-29dB)

• 173
(-54dB)

— 2° —

• 1929
(-12dB)

○ Zenith

☐ Normal to Array

• 257	• 316	• 811	• 3857	• 941	• 626	• 536
(-47dB)	(-43dB)	(-27dB)	(0dB)	(-25dB)	(-32dB)	(-34dB)

• 223
(-50dB)

• 837
(-27dB)

• 105
(-63dB)

— 2° —

• 1516
(-16dB)

• 841
(-26dB) ⊙ Zenith

• 1126
(-21dB) ⊞ Normal to Array

• 566
(-33dB)

• 3800
(0dB)

• 1116
(-21dB)

• 890
(-25dB)

• 624
(-31dB)

• 167
(-54dB)

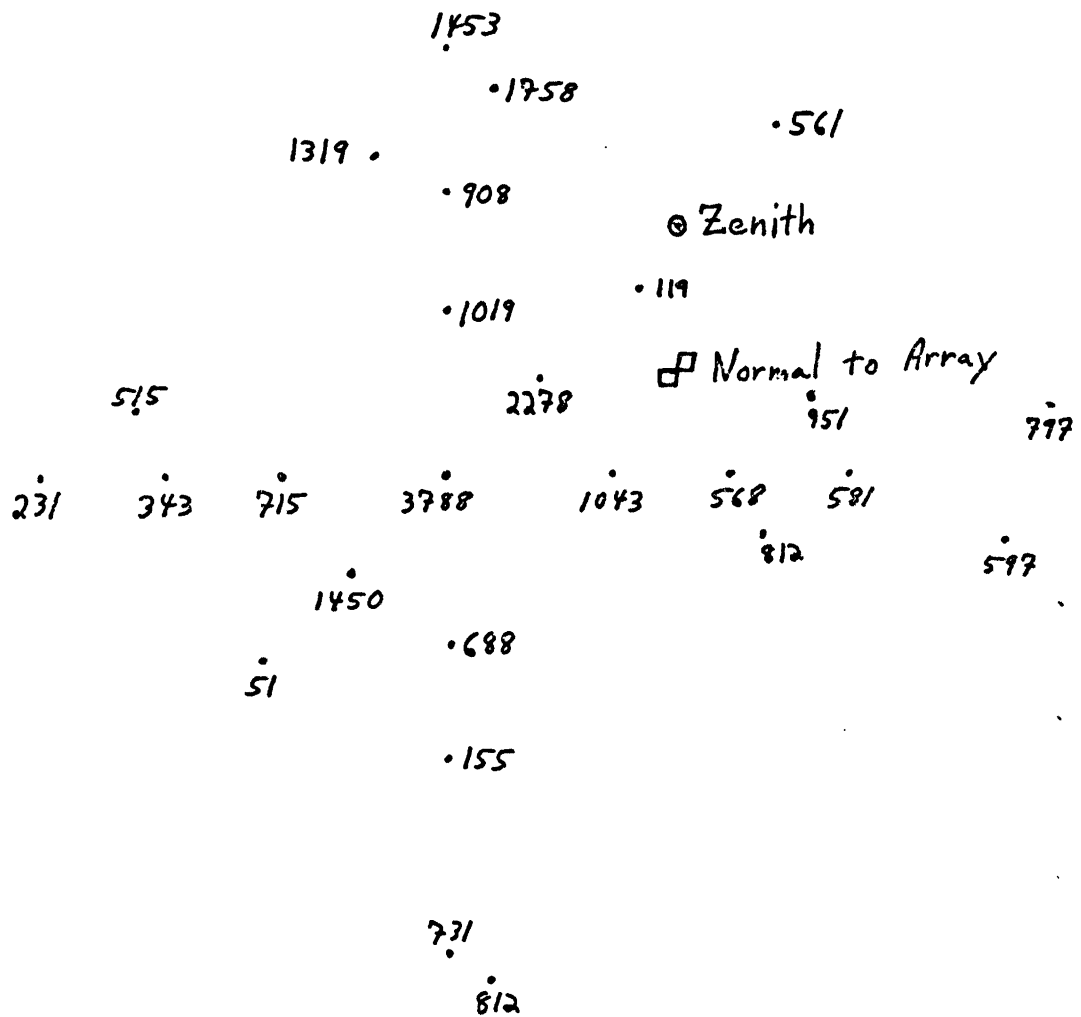
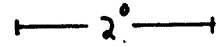
• 753
(-28dB)

Antenna Beam Map 5

The beam pattern may then be calculated once the cable insertions have been specified. The phase scheme

N_m		E_m
4325		
3254		
2543		
5432		
	5432	
	4325	
	3254	
	2543	
W_m		S_m

is often used in ionospheric scattering experiments, and is found to move the beam 2.33° along each axis. This is very close to the 2.31° shift along each axis achieved by the full antenna with comparable cable insertions. The advantage of this diagonal configuration is the narrow beam which results on the diagonal along which the quarters lie, and the availability of the remaining two quarters for a complementary measurement. Antenna Beam Map 6 reveals the fundamental problem with such a configuration, the large (-9dB) side lobe 1.4° away from the main lobe. A side lobe of this amplitude represents a substantial contribution to the returned signal from an unwanted scattering volume. This renders the "bow-tie" antenna unsuitable for use in stratospheric wind experiments,



Antenna Beam Map 6

BIBLIOGRAPHY

- Booker, H. G. and W. E. Gordon, A theory of radio scattering in the troposphere, Proc. IRE, 38, 401, 1950.
- Deer, V. E. (ed.), Remote Sensing of the Troposphere, U.S. Government Printing Office, Washington, D. C., 1972.
- Gordon, W. E., Incoherent scattering of radio waves by free electrons with applications to space exploration by radar, Proc. IRE, 46, 1824, 1958.
- Jasik, H. (ed.), Antenna Engineering Handbook, McGraw-Hill, New York, 1961.
- Kraus, J. D., Radio Astronomy, McGraw-Hill, New York, 1966.
- Kraus, J. D., Antennas, McGraw-Hill, New York, 1950.
- Ochs, G. R., The large 50 Mc/s array at Kicamarca radar observatory, U.S. Dept. of Commerce, National Bureau of Standards, NBS Rep. 8772, 1965.
- Rastogi, P. K., Remote Sensing of the Mesosphere using the Jicamarca Incoherent-Scatter Radar, Ph.D. Thesis, Univ. of Illinois, 1975,
- Tatarski, V. I., Wave Propagation in a Turbulent Medium, translated from the Russian by R. A. Silverman, McGraw-Hill, New York, 1961.
- Webb, W. L., Structure of the Stratosphere and Mesosphere, Academic Press, New York, 1966.
- Wheelon, A. D., Radio-wave scattering by tropospheric irregularities, J. Res. NBS, 63D, 205, 1959.
- Wheelon, A. D., Backscattering by turbulent irregularities: a new analytical description, Proc. IEEE, 60, 252, 1972.

Wolff, E. A., Antenna Analysis, John Wiley & Sons, New York, 1966.

Woodman, R. F. And A. Guillen, Radar observations of winds and turbulence in the stratosphere and mesosphere, J. Atmos. Sci., 31, 492, 1974.

Woodman, R. F. and T. Hagfors, Methods for the measurement of vertical ionospheric motions near the magnetic equator by incoherent scattering, J. Geophys. Res., 74, 1205, 1969.